

Report: Testing of the integrated heat pump

Public

Deliverable 2.4

May 2021



This project has received funding from the European Union's Horizon 2020 research and innovation programme under Grant Agreement No. 814865 (RES4BUILD). This output reflects only the author's view. The European Climate, Infrastructure and Environment Executive Agency (CINEA) and the European Commission cannot be held responsible for any use that may be made of the information contained therein.

Acknowledgements

This report has been produced as part of the project “Renewables for clean energy buildings in a future power system” or RES4BUILD for short.

This work has been carried out by:

| | | |
|-------------------------|---|--|
| WP | 2 | |
| WP, task number | 2.4 | |
| WP leader | DTU | |
| Responsible task leader | DTI | |
| Responsible partner | DTI | |
| Authors | DTI, DTU & NCSR | |
| Type of deliverable | Report [X] Prototype [] | Demonstrator [] Other [] |
| Dissemination level | Public [X] Prog. Participants [] | Restricted Designated Group [] Confidential (consortium) [] |

Disclaimer:



This project has received funding from the European Union’s Horizon 2020 research and innovation programme under Grant Agreement No. 814865 (RES4BUILD). This output reflects only the author’s view. The European Climate, Infrastructure and Environment Executive Agency (CINEA) and the European Commission cannot be held responsible for any use that may be made of the information contained therein.

While this publication has been prepared with care, the authors and their employers provide no warranty with regards to the content and shall not be liable for any direct, incidental or consequential damages that may result from the use of the information or the data contained therein. Reproduction is authorised providing the material is unabridged and the source is acknowledged.



ARUP



ThermoVault



Table of Contents

| | |
|---|-----------|
| ACKNOWLEDGEMENTS | 2 |
| EXECUTIVE SUMMARY | 5 |
| 1 INTRODUCTION AND HIGHLIGHTS OF THE HEAT PUMP TECHNOLOGIES | 10 |
| 1.1 THE VAPOUR COMPRESSION HEAT PUMP | 10 |
| 1.2 THE MAGNETOCALORIC HEAT PUMP | 12 |
| 2 VAPOUR COMPRESSION HEAT PUMP TESTING AT NCSR | 13 |
| 2.1 INTRODUCTION | 13 |
| 2.2 DESCRIPTION OF THE TESTING FACILITIES AT NCSR | 13 |
| 2.2.1 TEST-RIG CONFIGURATION | 15 |
| 2.2.2 TESTING CONDITIONS | 17 |
| 2.3 TEST RESULTS | 17 |
| 2.3.1 OPERATION DURING THE DAY | 17 |
| 2.3.2 RESULTS AT VARIOUS OPERATING CONDITIONS | 19 |
| 2.4 CONCLUSIONS AND ACTIONS TAKEN | 24 |
| 3 VAPOR COMPRESSION HEAT PUMP TESTING AT DTI | 25 |
| 3.1 TEST SETUP | 25 |
| 3.1.1 STABIL HEAT PUMP OPERATION | 26 |
| 3.2 TEST RESULTS | 26 |
| 3.2.1 CONTINUATION OF TESTS | 27 |
| 4 THE MAGNETOCALORIC HEAT PUMP IN THE INTEGRATED HEAT PUMP | 28 |
| 4.1 INTRODUCTION | 28 |
| 4.2 CHALLENGES IN THE TESTING OF THE MAGNETOCALORIC HEAT PUMP | 29 |
| 4.3 VIRTUAL INTEGRATION OF THE MAGNETOCALORIC HEAT PUMP | 30 |
| 4.3.1 INTEGRATION STRATEGIES | 30 |
| 4.3.2 VIRTUAL INTEGRATION | 31 |
| 5 RESULTS FOR THE INTEGRATED HEAT PUMP | 32 |
| 5.1 METHOD FOR INTEGRATION | 32 |
| 5.2 EVALUATION OF TEST RESULTS FOR THE INTEGRATED HEAT PUMP | 32 |
| 6 MODIFYING THE HEAT PUMP FOR ENHANCING THE RES4BUILD SYSTEM PERFORMANCE | 34 |
| 6.1 EVALUATION OF HEAT PUMP TEST RESULTS AND NECESSARY MODIFICATIONS | 34 |

| | | |
|------------|---|-----------|
| 6.1.1 | EVALUATION OF TEST RESULTS AND COMPRESSOR EFFICIENCY | 34 |
| 6.1.2 | MODIFICATIONS FOR INCREASING THE PERFORMANCE | 40 |
| 6.1.3 | NUMERICAL MODEL OF THE IMPROVED HEAT PUMP | 41 |
| 6.2 | RES4BUILD SYSTEM PERFORMANCE | 43 |
| 6.2.1 | SYSTEM OVERVIEW AND OPERATING MODES | 43 |
| 6.2.2 | HEATING AND COOLING DEMAND | 44 |
| 6.2.3 | PARAMETERS AND CASES EXAMINED | 46 |
| 6.2.4 | MONTHLY RESULTS | 46 |
| 6.2.5 | ANNUAL RESULTS AND COMPARISON WITH CONVENTIONAL SOLUTIONS | 48 |
| 7 | CONCLUSION AND NEXT STEPS | 50 |

Executive Summary

This report describes the work and results of task 2.4 “Testing of the integrated multi-source heat pump” in the RES4BUILD work package 2.

The main purpose of task 2.4 is to test the vapour compression heat pump in order to characterize the performance and to measure the efficiency. Afterwards, the intention was to couple the vapour compression heat pump with the magnetocaloric heat pump made by the Technical University of Denmark (DTU) in a cascade coupling, as defined in D2.2, and to test the integrated heat pump focusing on its overall efficiency. Later on, the integrated heat pump will be the central component of the pilot system constructed at Danish Technological Institute (DTI) where solar PV and solar thermal heat production from the PVT collectors along with virtual borehole thermal energy storage (BTES) are included in a “real-time” test system, which simulates realistic heat consumption profiles.

Heat pump tests

The vapour compression heat pump was designed and produced by Psycrotherm in Greece according to the simulation results achieved in task 2.3. It was initially tested at Demokritos National Centre for Scientific Research (NCSR).

At NCSR, the functionality of the heat pump including the control software, valve functions, and measurements were tested. Afterwards, an extended test programme was carried out. This involved variable evaporator and condenser temperatures, variable compressor frequencies, and variable water flow rates.

The heating capacity of the heat pump was in the range of 4 kW to 11 kW depending on the temperature increase. The highest temperature increase of 45 K resulted in a heating capacity of 4 kW.

The heat pump COP (the heating efficiency) is strongly dependant on the evaporator and condenser temperatures. The system COP, including auxiliaries, is shown in Fig.1 for various evaporator temperatures as a function of the condenser temperature.

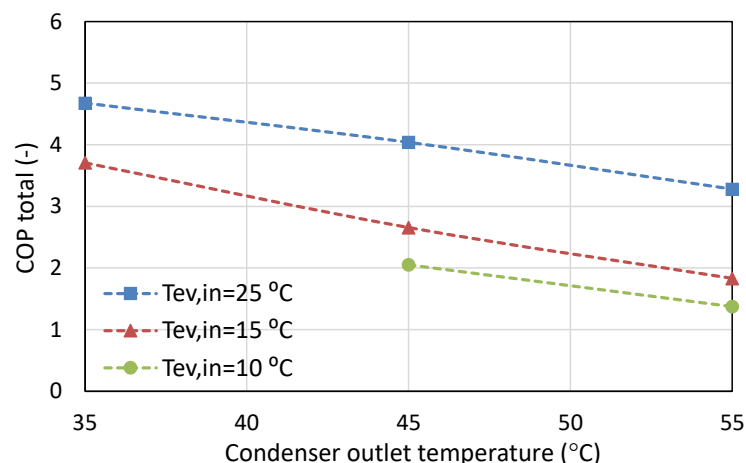


Fig. 1. Measured vapour compression heat pump COPs with variable evaporator and condenser temperatures from tests at NCSR

After a few improvements made by Psycrotherm, the heat pump was shipped to DTI for further testing.

Initially, it was challenging to achieve stable heat pump operation because the condenser water outlet temperature fluctuated significantly. After a process of troubleshooting, a replacement of the thermostatic expansion valve, and a refilling of the refrigerant of the heat pump, stable operating conditions were achieved.

The following results were achieved at DTI with variable temperatures in the evaporator and the condenser:

Table 1: Measured vapour compression heat pump COPs from tests at DTI

| Evaporator water inlet temp. [°C] | Condenser water outlet temp. [°C] | | |
|--|--|-----------|-----------|
| | 35 | 45 | 55 |
| 5 | 2.21 | 1.17 | 0.93 |
| 15 | 3.73 | 2.66 | 1.63 |
| 25 | 5.17 | 4.09 | 3.07 |

Meanwhile, the magnetocaloric heat pump tests at DTU achieved a COP of 6.7 at a temperature increase of 11.6 K, which is described in the RES4BUILD deliverable 2.1 report. However, the tests at DTU also showed that the operation of the magnetocaloric heat pump is sensitive due to the innovative character of the technology. Therefore, transporting the heat pump from DTU in Lyngby, Denmark, to DTI in Aarhus, Denmark, would include a high risk of difficulties in making the magnetocaloric heat pump operate at stable conditions, especially when the magnetocaloric heat pump is to operate in a cascade coupling with the vapour compression heat pump. Based on these test experiences, it was decided not to move to magnetocaloric heat pump from DTU.

Instead, the coupling of the two heat pumps will be performed virtually. The overall efficiency of the integrated heat pump was calculated by combining the efficiencies of the two heat pumps.

In the test of the pilot system in work package 5, the magnetocaloric heat pump will be simulated by including an electrical heater, which represents the magnetocaloric heat pump. Here, the efficiency from the testing at DTU will be considered in order to extract the system performance.

Based on the current status of the two heat pumps, the overall integrated COP was calculated from the results from the vapour compression heat pump test and the magnetocaloric heat pump test.

Table 2: Calculated efficiencies of the integrated heat pump based on test values

| Temperature span | Calculated overall COP based on test results | Calculated Carnot efficiency |
|------------------|--|------------------------------|
| 5°C - 55°C | 1.75 | 27 % |
| 5°C - 45°C | 2.26 | 28 % |
| 5°C - 35°C | 2.76 | 27 % |

The efficiencies of the integrated heat pump were lower than expected and they were lower than existing heat pump solutions on the market. This is partly because of the high innovative level of the magnetocaloric heat pump, where further development potential still remains. The performance of the vapour compression heat pump was also lower than existing market levels. In work package 5, further developments will be carried out in order to increase the efficiency of the vapour compression heat pump as highlighted in the following.

Improvements towards increasing the system COP

Although improvements have been done by Psycrotherm before the vapour compression heat pump was shipped to DTI in September 2020, the performance was still lower than expected as is revealed from the test results. The main reason for this is the under-performing scroll compressor, which operates at a lower pressure with the selected refrigerant R1234ze(E). To better understand the main source of losses within the compressor, a semi-empirical model has been developed, which revealed that the suction pressure drop is very high leading to a reduced mass flow rate and a very low volumetric and isentropic efficiency.

Based on these outcomes and once the heat pump tests at DTI had been finished and all the results had been evaluated, it was decided to replace the compressor and the refrigerant in order to improve the performance of the heat pump and to challenge the performance of high-efficiency commercial products based on HFC refrigerants. In order to do so, the heat pump will be shipped back from DTI to Psycrotherm in May 2021 for the handling of these modifications.

At the same time, an evaluation of alternative compressors/refrigerants has been initiated, mostly focusing on a new series of scroll compressors suitable for HFO blends, which were released at the beginning of 2021. A comparative analysis of the different combinations of compressors and refrigerants has then been performed based on the specifications provided by the compressor manufacturer with typical suction superheat and subcooling parameters. The initial screening identified a scroll compressor with the refrigerant R454C (an HFO blend with a GWP of 148), while the final selection will be conducted within Task 5.3. Once Psycrotherm receives the heat pump from DTI, they will proceed with the necessary modifications to the heat pump during the summer of 2021. Subsequently, tests will then be carried out by both Psycrotherm in Greece and DTI in Denmark to verify the performance of the heat pump. This activity will be presented in deliverable D5.3.

According to the performance indicators of the compressor manufacturer, an equation-fitting procedure has been conducted by NCSR in order to produce a suitable model, which is to be used in the system simulations using the numerical tools developed in Task 3.1. The produced performance maps concern correlations that provide the heat flows, the electricity consumption, and the COP as a function of water and air temperatures for water-source and air-source operation, respectively.

This heat pump model has been used in the system simulations together with PVT collectors for producing heat and electricity and the multi-source heat pump for heating and cooling, once coupled with a BTES field. The system is intended to cover the space heating/cooling and domestic hot water (DHW) demand of a multi-family residential building. The heating and cooling modes are illustrated in Fig. 2, along with the main system components, their connections, and the heat source and sink options.

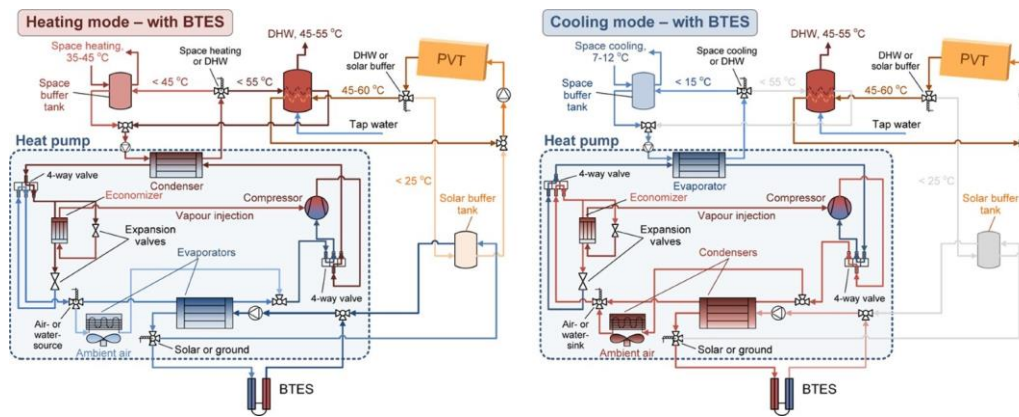


Fig. 2. System layout with the PVT collectors, the multi-source heat pump, the BTES, and the three water tanks. Left: Heating mode, Right: Cooling mode

The annual simulations have been conducted for the same building in Athens, Greece, with both heating and cooling needs and in Copenhagen, Denmark, with only heating needs. The processing of the numerical results provided the monthly average COP for space heating, DHW, and space cooling at both locations. These results are presented in Fig. 3.

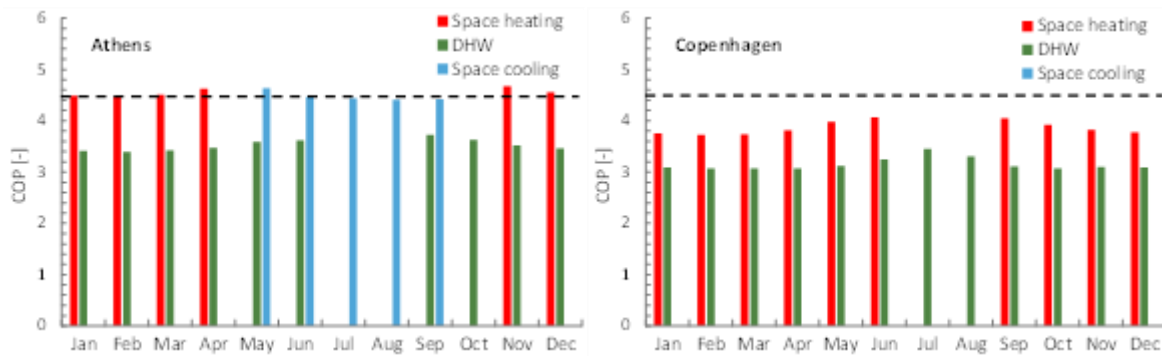


Fig. 3. Monthly averaged COP of the RES4BUILD system in Athens and Copenhagen

The COP for space heating and space cooling in Athens is about 4.5 during all months, while it is lower for DHW due to the higher supply temperature to the water tank. In comparison, the COP in Copenhagen is kept at a lower value due to the reduced ground temperature, which is about 10 K lower than the one in Athens.

The seasonal COP of the heat pump unit is 4.29 in Athens and 3.61 in Copenhagen, where the contribution of the heat collectors is lower. The COP per mode is presented in Table 3.

Table 3. COP per mode at the two locations

| Mode | Heat pump COP (-) | |
|-----------------------|-------------------|-------------|
| | Athens | Copenhagen |
| Space heating | 4.53 | 3.81 |
| Space cooling | 4.45 | - |
| DHW | 3.46 | 3.12 |
| Total seasonal | 4.29 | 3.61 |

By considering the produced PVT electricity, which is comparable with the system electricity consumption during the summer months, it is possible to extract the primary energy demand. This demand is then compared to the one of a conventional system with a gas boiler and standard split air-conditioning units. The results show that the RES4BUILD system reduces more than four times the primary energy demand of the heating/cooling system of the residential building in Athens and two times more in Copenhagen due to the effective combination of renewable energy systems.

It should be stressed that the positive effect of the optimisation tools of WP3 is not taken into consideration, which further reduces the primary energy demand. This will be included in the different case studies over a wider range of building types and locations which will be conducted in Task 7.1 to identify the impact of the RES4BUILD solution.

1 Introduction and highlights of the heat pump technologies

The primary focus of work package 2 is to produce and test a highly effective and innovative integrated heat pump consisting of a magnetocaloric heat pump combined with a vapour compression heat pump in a cascade coupling. The magnetocaloric heat pump will provide the low temperature increase and the vapour compression heat pump will provide the following temperature increase producing hot water sufficient for space heating and domestic hot water (DHW).

In work package 5, which will continue to April 2023, the integrated heat pump will be installed and tested in a pilot system with solar thermal and PV as well as virtual borehole thermal energy storage.

The magnetocaloric heat pump has been manufactured and tested at the Technical University of Denmark (DTU). The vapour compression heat pump has been manufactured at Psycrotherm in Greece and tested at Demokritos National Centre for Scientific Research (NCSR). Afterwards, it was sent to Danish Technological Institute (DTI) for final testing and integration with the magnetocaloric heat pump.

1.1 The vapour compression heat pump

One of the main requirements of the magnetocaloric heat pump is the use of a very high water flow rate. This leads to a very low temperature difference at the evaporator side of the vapour compression heat pump, which is supplied with heat from the hot side of the magnetocaloric heat pump. This aspect has been introduced in the simulations of the integrated heat pump that aided the vapour compression heat pump design (presented in deliverable D2.2).

Except from that, one of the biggest challenges of the design process of the vapour compression heat pump was the compressor selection, since there was not any available with an eco-port for the selected HFO refrigerant, R1234ze(E). After communications with different OEMs, it was decided to use a Copeland scroll compressor, type ZH13¹, concluding to a maximum heating capacity of about 11 kW. Once the compressor has been identified, Psycrotherm proceeded with the design of the complete heat pump and the selection of all its parts, with special focus on being compatible with the refrigerant. Pressure and temperature sensors have been mounted on the refrigerant and water piping for a detailed verification of the properties of the fluids and to assist in the numerical model validation. The control software of the PLC unit of the heat pump has also been prepared, which takes into account the different modes (e.g. air-source or water-source) and includes all safety measures and settings. The final design of the RES4BUILD vapour compression heat pump is shown in Fig. 1.1.

¹ Copeland scroll compressor, ZH series: <https://climate.emerson.com/en-gb/shop/1/copeland-eu-copeland-scroll-zhkve-compressors-en-gb?fetchFacets=true#facet:&facetLimit:&productBeginIndex:0&orderBy:2&pageView:list&minPrice:&maxPrice:&pageSize:&>.

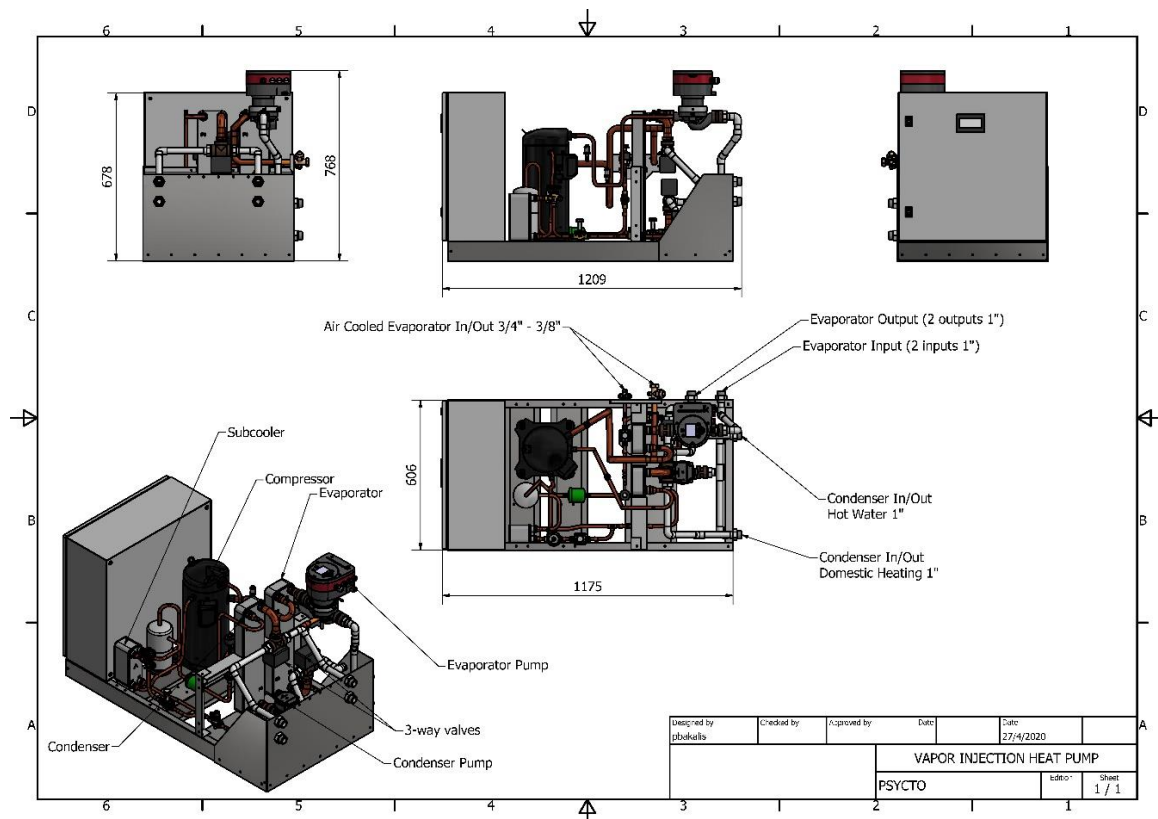


Fig. 1.1. Final design of the vapour compression heat pump with vapour injection

After that, Psycrotherm started by purchasing all components and installing them in a steel structure that offered significant space for changes, in case this was needed. An air-source evaporator has also been designed and produced by Psycrotherm, since the heat pump is able to adjust its heat source to either air or water. Figure 1.2 shows the heat pump at the last stages of its production, when all components/parts have been installed and connected.

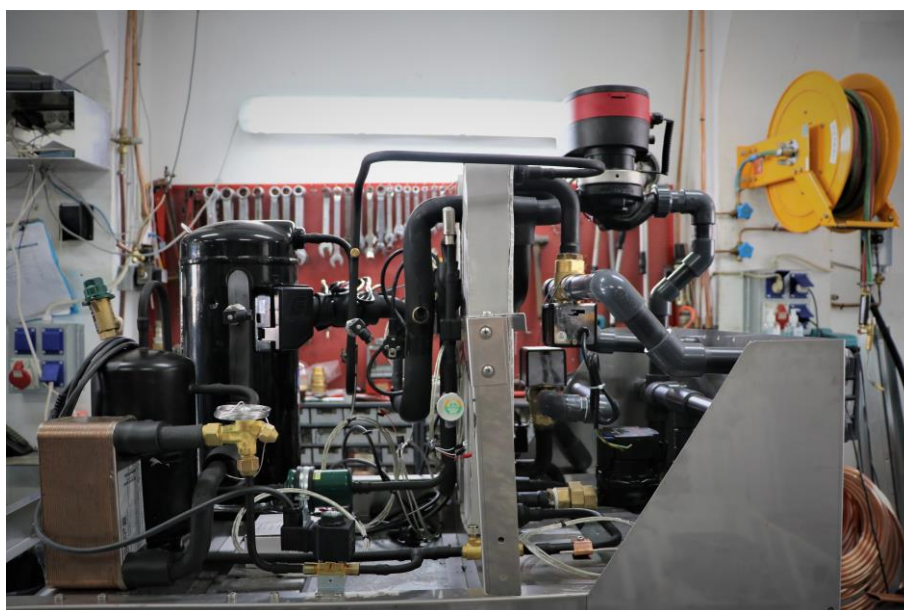


Fig. 1.2. The heat pump at the last stages of production

The heat pump production was finalized in May 2020 and after supervising the electrical connections and all sensors, it was shipped to NCSR D for the initial lab testing. The description of the initial tests and their results will be presented later in this report. Once these tests have been completed, the heat pump was returned to Psycrotherm for further improvements in order to:

- Increase the COP, by (1) improving the insulation at the hot parts of the cycle (discharge and liquid/eco lines), and (2) replacing the single-phase compressor with the same model, but with a three-phase motor.
- Adjust the control software of the PLC unit by adding Modbus communication features so that it will be ready to be coupled with the Thermovault BEMS system since this heat pump will be at the center of the overall control of the pilot system at DTI in WP5.

1.2 The magnetocaloric heat pump

A large-scale magnetocaloric heat pump has been developed at DTU. It includes a two-pole magnet assembly delivering an average magnetic field of 1.46 T into 13 regenerator beds containing the magnetocaloric material. The heat pump makes use of the magnetocaloric effect, which causes the magnetocaloric material to become warm by increasing the applied magnetic field and to cool down by decreasing the magnetic field. A laminated iron ring is used to direct the magnetic flux into the desired regenerator beds. Each regenerator bed is filled with ten different alloys of LaFeSiMnH, obtained from Vacuumschmelze GmbH in Germany. The layers have transition (active) temperatures in the range of 2°C to 22°C and are layered successively. This means that the temperature span of the heat pump must be held within this range to obtain an efficient heat pump operation.



Fig. 1.3. Magnetocaloric heat pump developed at DTU Energy

The magnetocaloric heat pump was tested at DTU and the results are reported in the RES4BUILD D2.1 “Development and Testing of the Magnetocaloric Heat Pump” report.

Due to the operational sensitivity of the magnetocaloric heat pump it was decided to do a virtual integration of the two heat pumps where the magnetocaloric heat pump would not be sent to DTI for testing.

2 Vapour compression heat pump testing at NCSR D

2.1 Introduction

The main aim of the heat pump testing that has been performed at NCSR D is to verify its reliability and evaluate the operational flexibility. Especially the latter is critical in the pilot system, when adjusting the heat source temperature over a large range or shifting from air-source operation to water-source. These tests were also important for debugging the control algorithms of the vapour compression heat pump and fixing the safety measures of the unit (e.g. in case of refrigerant loss, frost formation at the air-fan, or overheating).

These tests have been conducted at the Solar & other Energy Systems Laboratory (SESL) of NCSR D during the summer of 2020. Once these finished, NCSR D and Psycrotherm conducted a preliminary assessment of the results, leading to some additional improvements to the heat pump such as replacing the single-phase compressor with the same three-phase one, and better insulation at the high-temperature parts of both the water and refrigerant circuit. After that, Psycrotherm shipped the vapour compression heat pump to DTI in September 2020 for the final tests and integration with the magnetocaloric heat pump of DTU.

The report presents the testing facilities and the main test data that have been obtained. The latter have been evaluated and led to the improvements mentioned above, which proved not to be sufficient for reaching a high performance.

2.2 Description of the testing facilities at NCSR D

The heat pump was delivered to NCSR D in June 2020. It has been installed in the facilities of the Solar & other Energy Systems Laboratory, where temperature-controlled hot or chilled water flow is available. The air-fan has been placed indoors, as shown in Fig. 2.1, since the outdoor ambient temperature was always above 30 °C during the day and did not allow the air-source operation.

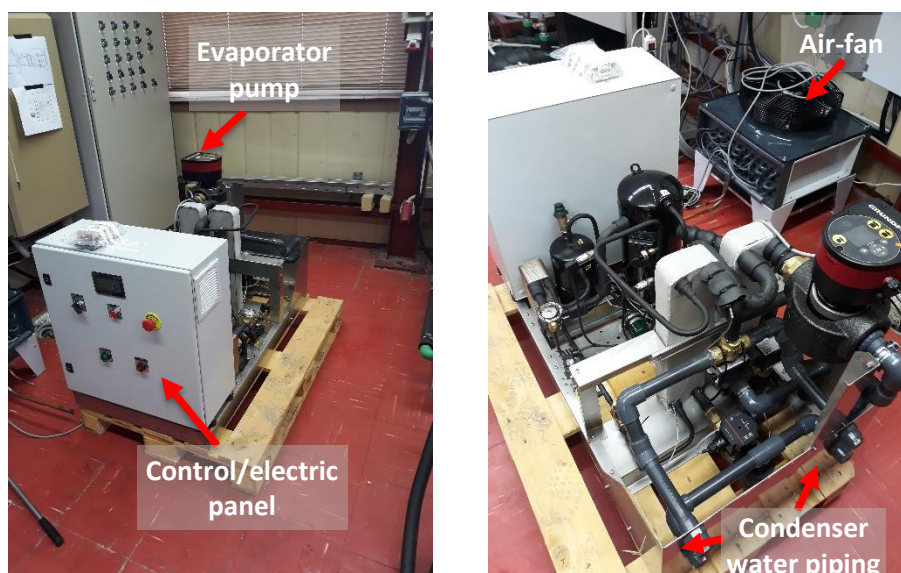


Fig. 2.1. Heat pump at the NCSR D lab with the air-fan placed indoors

The connections have then been conducted at the refrigerant and water piping and charging the heat pump with 4 kg of the selected HFO refrigerant, R1234ze(E). The refrigerant piping connecting the air-fan is shown at the left in Fig. 2.2 and the hydraulic connections at the right.



Fig. 2.2. Left: Refrigerant connections and charging the heat pump. Right: Hydraulic connections with temperature sensors

The measurements that are collected at the water and air side are the inlet/outlet temperature and flow rates at the evaporator and condenser, the (indoor) ambient temperature, and the total power consumption. The meters/sensors that are used for that purpose at the condenser side are shown in Fig. 2.3.

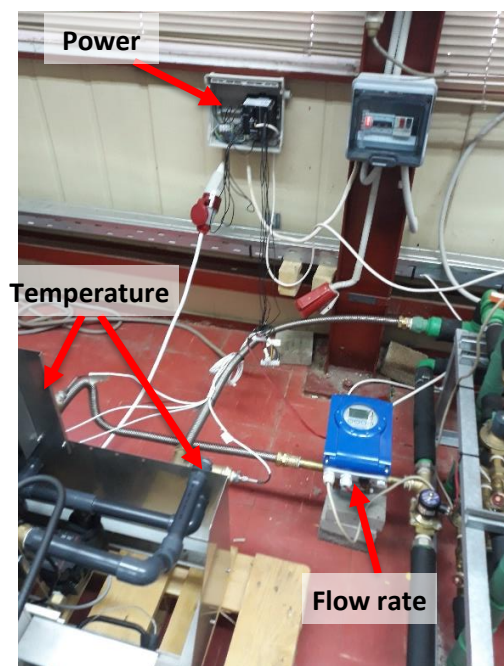


Fig. 2.3. Measurements of the heat pump

These measurements are collected and recorded by a data logger with a sampling rate defined by the user. For the current tests, this rate is once every 30 seconds. The measurements are visualized in a computer screen at real-time in order to directly identify any malfunction.

Except from the power and water-side measurements, the heat pump itself is equipped with temperature and pressure sensors at various parts of the piping. These measurements are collected and recorded by the PLC unit of the heat pump with a sampling rate of one minute.

All sensors and meters have been calibrated and are shown in Table 2.1, providing the measurement range and their accuracy as well.

Table 2.1. Sensors and meters of the heat pump

| Meter/sensor | Quantity | Type | Range | Accuracy |
|-------------------------------|----------|---|---|-------------|
| Lab side | | | | |
| Water flow meter (condenser) | 1 | Yokogawa ADMAG AXF electromagnetic flow meter | Adjustable (0-20,000 lt/h) | <1% |
| Water flow meter (evaporator) | 1 | Krohne IFC 010D electromagnetic flow meter | Adjustable (0-15,000 lt/h) | <1% |
| Water temperature | 4 | PT100, 4-wire | 0-100 °C | 0.1 K |
| Power meter | 1 | Siemens Sicam-T | 0-50 kW per phase (with current transformers) | 0.5% |
| Heat pump side | | | | |
| Refrigerant temperature | 6 | PT100 | -200 – 850 °C | 0.1 K |
| Refrigerant pressure | 3 | Pressure transmitter ESCP-MIT1 | Up to 30 bar | 0.25% of FS |
| Water temperature | 4 | PT100 | -200 – 850 °C | 0.1 K |

Except from the above, the heat pump inverter records the compressor consumption (and the air-fan when it operates, since they are both driven by the same inverter) and frequency. These measurements along with the refrigerant and water properties are saved in a SD card as .csv files in the electric panel of the heat pump for further processing.

2.2.1 Test-rig configuration

The hot and cold side of the heat pump are connected to a different water tank (each of 5 m³). The evaporator is connected to a tank (“cold tank”) that is equipped with electric resistances for heating up the stored water (three resistances of 9 kW each, similar to the evaporator heat). On the other hand, the condenser is connected to a second tank (“hot tank”) that is equipped with an air-source heat pump for chilling the stored water. By doing so, the inlet water temperature to the heat pump can be stabilized at both the evaporator and condenser, allowing to perform tests with a high duration at almost constant supply conditions. With rough estimations, the water tank temperature is increased or reduced by 1.5 K every hour of full load operation of the heat pump. Each tank has a circulation pump for recycling the water from the top to the bottom and thus de-stratify the stored water. The two tanks are shown in Fig. 2.4, with the RES4BUILD heat pump installed just inside the building.

2.2.2 Testing conditions

Most of the tests have been performed with water, since the indoor temperature could not be controlled over a large range and thus identify the air-source heat pump performance. The operation of the heat pump with the air evaporator has been tested during a single day with an ambient temperature of about 23 °C and the condenser output in the range of 40-45 °C.

All other tests have been performed with water. The evaporator inlet temperature ranged from 10 °C up to 25 °C, while the condenser outlet ranged from 32 °C up to 55 °C. Regarding the tests at different hot/cold temperatures, three main sets have been conducted with the compressor running at 50 Hz, highlighted next:

1. Constant evaporator inlet temperature of 25 °C and sweep the condenser output up to 55 °C.
2. Constant evaporator inlet temperature of 15 °C and sweep the condenser output up to 55 °C.
3. Constant evaporator inlet temperature of 10 °C and sweep the condenser output up to 55 °C.

It was not possible to further reduce the evaporator temperature down to 5 °C, since the cold tank is placed outdoors and there were high heat losses from the piping and the tank (outdoor ambient temperature always over 30 °C).

At the beginning of every set, the heat pump was operating in order to bring the cold tank to the desired temperature level. At the same time, however, the hot tank was heated, and it was necessary to switch-on the external heat pump for reducing its temperature. This procedure was repeated three times and each one lasted for about 1-2 days.

During each of the above tests, the temperature of the cold tank supplying the evaporator was stabilized by switching on/off the electric resistances. The hot tank temperature was then continually increased until it reached the maximum temperature set-point, equal to 55 °C.

The above tests have been conducted for constant water flow rates (1.35 m³/h at the condenser and 2.18 m³/h at the evaporator) and a compressor frequency of 50 Hz. After that, some short tests followed for a constant hot/cold temperature, but with variable water flow rates at both the condenser and evaporator and a reduced frequency up to 30 Hz.

2.3 Test results

2.3.1 Operation during the day

The heat pump was operating for the whole day, recording all measured data, and controlling the water temperature in the two tanks. A sample of such operation is given in Fig. 2.6, showing the inlet/outlet water temperatures from the condenser and evaporator during five hours of testing. The compressor operates at 50 Hz and the water flow rates are constant and equal to 1.35 m³/h at the condenser and 2.18 m³/h at the evaporator.

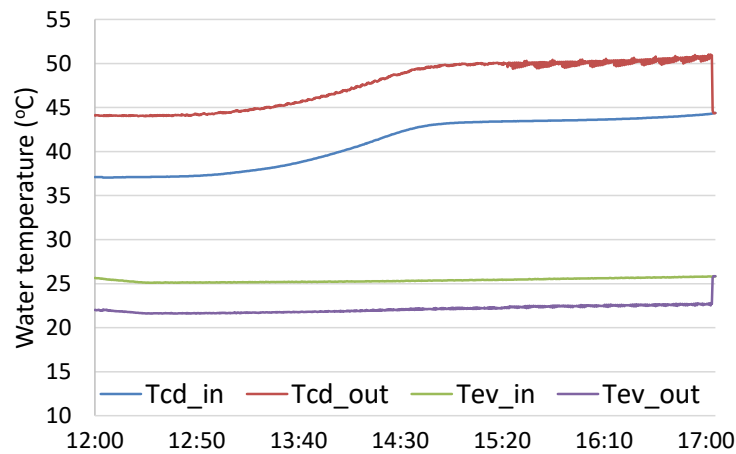


Fig. 2.6. Inlet/outlet water temperatures at the evaporator and condenser during the day

This case corresponds to the first testing case (inlet water temperature at the evaporator of 25 °C) with the temperature difference at the evaporator being 2-3 K. The evolution of the condenser water inlet temperature is identified as the result of the tank temperature that is increasing during the course of the testing.

The heat flows and electricity consumption during the same period are shown in Fig. 2.7. The electricity is the total one (P_{tot}) that includes the consumption of the two water pumps and all auxiliaries and control equipment (power consumption of pumps and auxiliaries is about 140 W).

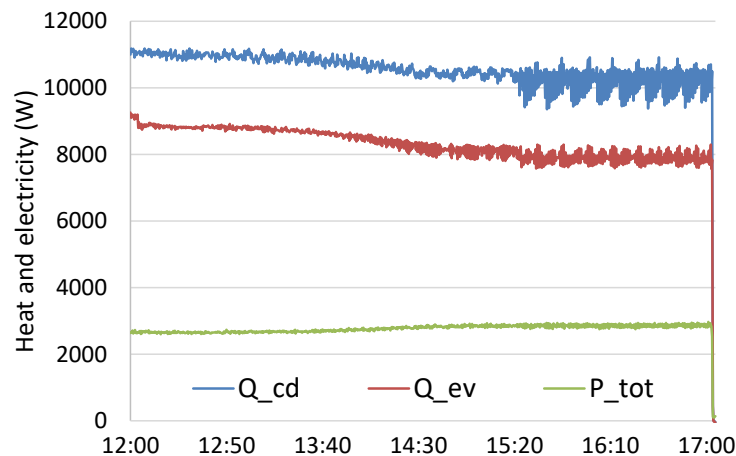


Fig. 2.7. Condenser and evaporator heat and total electricity consumption of the heat pump during the day

The condenser heat reaches the maximum capacity of 11 kW at the beginning of this period and then decays due to the increase of the condenser temperature. The evaporator heat follows exactly the same trend, while the electricity consumption increases from 2.5 kW to almost 3 kW due to the higher pressure ratio. The fluctuations during the last 2.5 hours of the testing period are due to the operating settings of the electronic expansion valve that is based on a PID control. This has been adjusted in the next tests at DTI, leading to a more stable operation.

The resulting COP is 4.8 during the beginning of this period and it then drops to about 4.2. Once the condenser temperature further increases and becomes 50 °C, the COP further drops to about 3.7. In case the power consumption of all pumps and auxiliaries is excluded, the compressor COP is initially around 5 and then it reduces to 3.8.

This kind of tests is useful to identify the response of the heat pump at varying temperatures and loads as well as to spot any operational issues that need to be resolved or any settings improved. This improvement and optimisation process is continuous and took place not only during the first tests at NCSR D, but also later on at DTI.

The testing period lasted for 19 days during June-July 2020 and the results have been processed, after their averaging every 10 minutes. Due to their large number, the main ones are presented in the next section that provides the performance and energy flows at key operating conditions.

2.3.2 Results at various operating conditions

2.3.2.1 Variable condenser and evaporator temperatures

The presentation of the test results begins with the variable condenser and evaporation water temperatures. The heat flows at the condenser and evaporator and the total electricity consumption of the heat pump for a variable condenser temperature and three representative water temperature levels at the evaporator inlet ($T_{ev,in}$) are presented in Figs. 2.8-2.10.

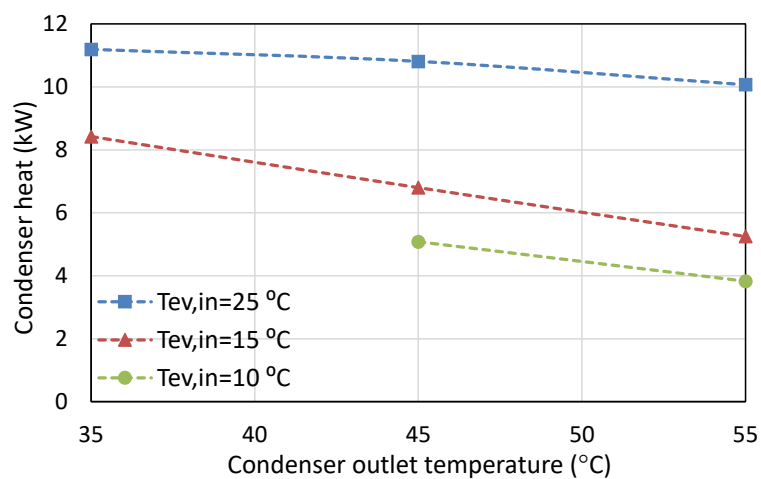


Fig. 2.8. Condenser heat for a variable condenser temperature and three water temperature levels at the evaporator inlet

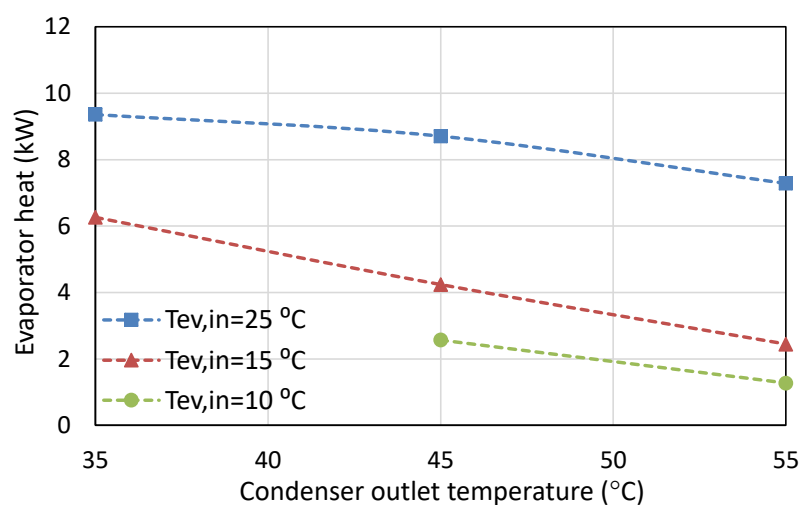


Fig. 2.9. Evaporator heat for a variable condenser temperature and three water temperature levels at the evaporator inlet

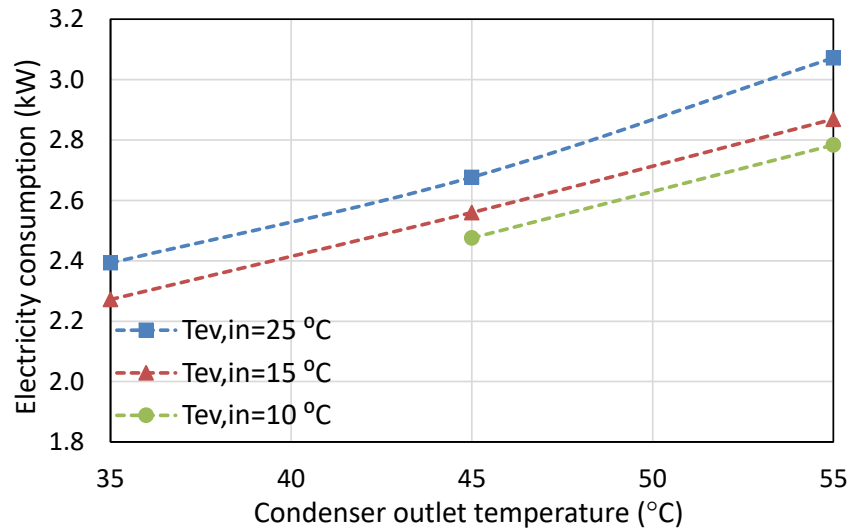


Fig. 2.10. Total electricity consumption for a variable condenser temperature and three water temperature levels at the evaporator inlet

The maximum heating capacity is about 11 kW, which has been obtained for a very low temperature lift of 10 K, with the minimum capacity of 4 kW for the maximum lift of 45 K. The electricity consumption for the same lift is reduced, indicating that the compressor operates with a high efficiency under an elevated pressure ratio, which is assisted by the presence of the vapour injection.

The overall heat pump performance is expressed through the COP, for which two separate values are given; one that includes the total electricity consumption with all auxiliaries (“total COP”) and another one with only the consumption of the compressor and any inverter losses (“compressor COP”). The power consumption of the auxiliaries (e.g. two water pumps) is about 140 W. The total COP and the compressor COP are presented in Figs. 2.10-2.11 for the same range of operating conditions.

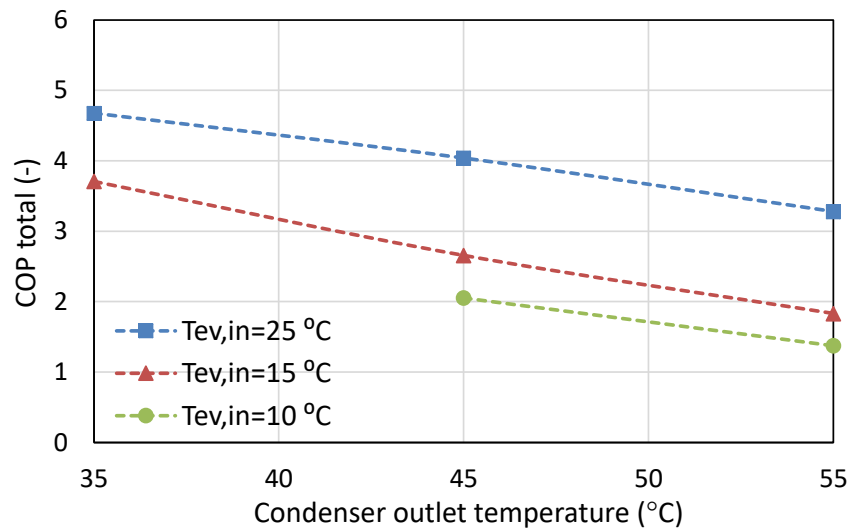


Fig. 2.11. System COP for a variable condenser temperature and three water temperature levels at the evaporator inlet

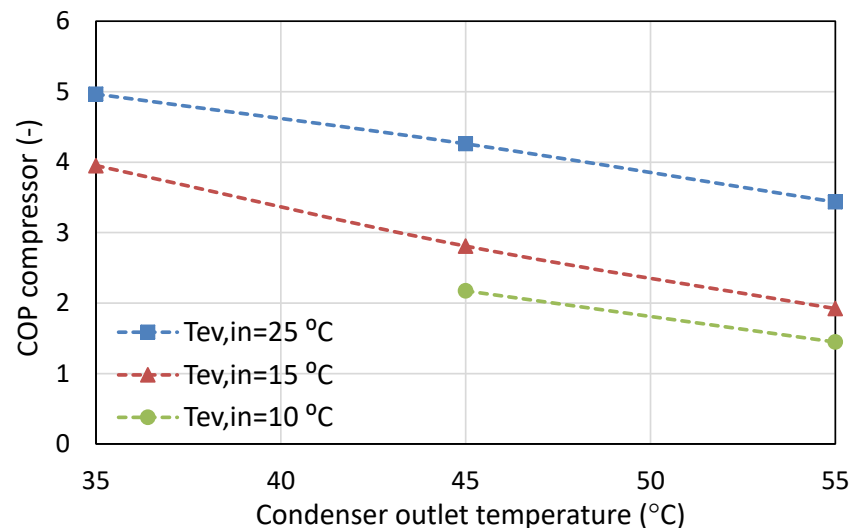


Fig. 2.12. Compressor COP for a variable condenser temperature and three water temperature levels at the evaporator inlet

The heat pump reaches a maximum COP of 5 for a low lift of 10 K, whereas for a lift of 20 K it is about 4 for all condenser temperatures. For a constant evaporator inlet temperature, the COP almost linearly decreases as the condenser temperature increases, as expected.

2.3.2.2 Variable compressor frequency

Except from the above tests at different water temperature levels at the evaporator and condenser, additional ones have been performed for a variable compressor speed.

The heat flows and (total) electricity consumption of the heat pump for a variable compressor frequency in the range of 30-50 Hz are presented in Fig. 2.13, whereas the resulting COP is depicted in Fig. 2.14. These tests have been performed for a constant evaporator and condenser water temperatures of 23 and 52 °C, respectively.

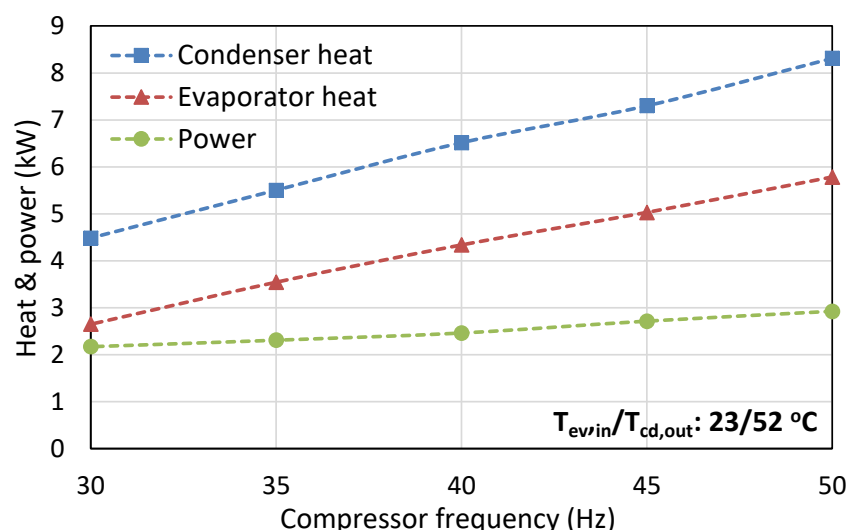


Fig. 2.13. Heat flows at the evaporator and condenser and electricity consumption of the heat pump for a variable compressor frequency

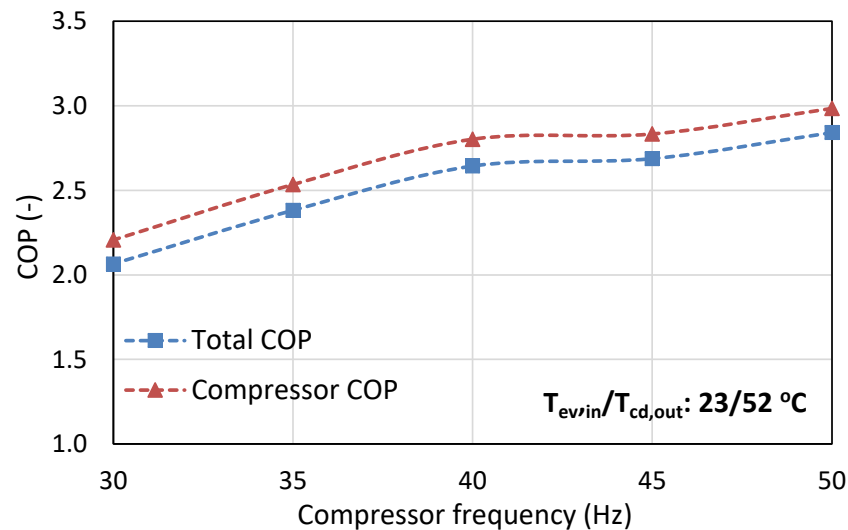


Fig. 2.14. Total and compressor COP of the heat pump for a variable compressor frequency

For the compressor with the single-phase motor that has been used in these tests, it is beneficial in terms of performance to operate at full speed that corresponds to 50 Hz. The COP is kept at high values up to 40 Hz and then it drops significantly. At the lowest frequency limit of 30 Hz, the COP is reduced by about 25% compared to the full speed operation.

2.3.2.3 Variable water flow rates

Next, the compressor frequency was set to 50 Hz and the condenser water flow rate was varied from 1.35 m³/h (the reference one used in all previous cases) until about 0.89 m³/h. The heat flows, electricity consumption, and COP values for variable condenser water flow rate are depicted in Figs. 2.15-2.16.

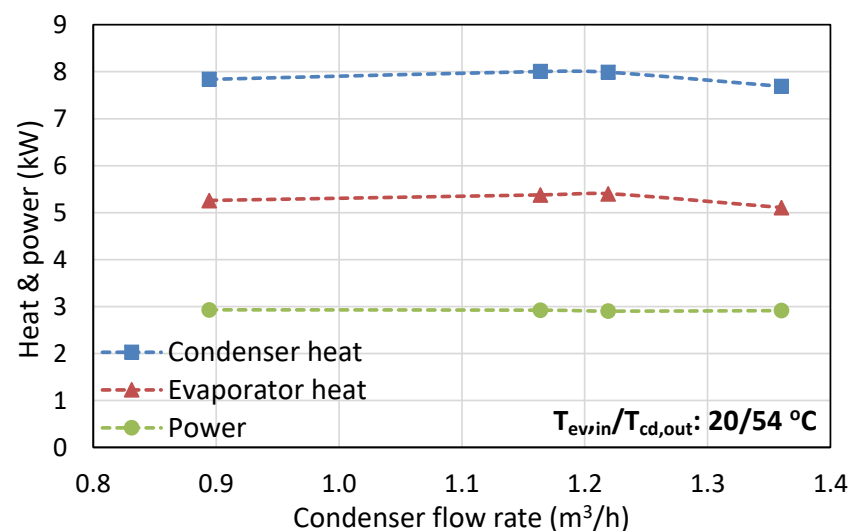


Fig. 2.15. Heat flows at the evaporator and condenser and electricity consumption of the heat pump for a variable condenser water flow rate

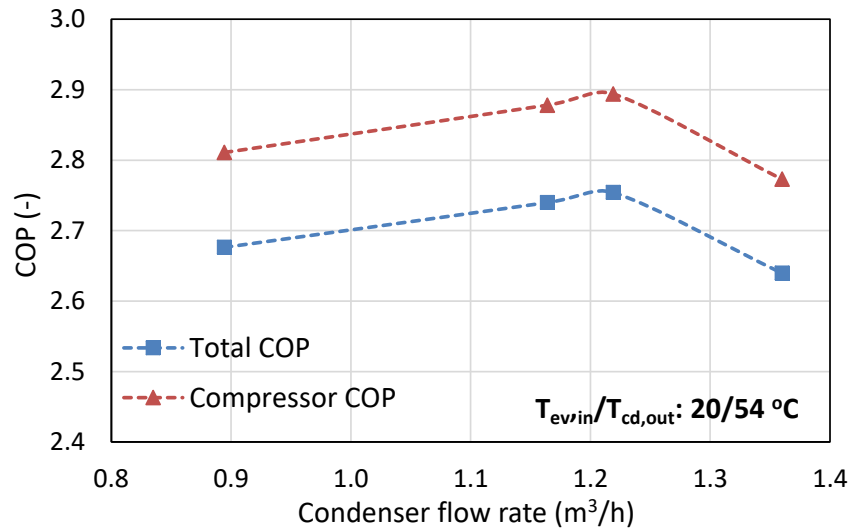


Fig. 2.16. Total and compressor COP of the heat pump for a variable condenser water flow rate

The variation of the condenser water flow rate introduces minor changes to the heat pump performance. The heat flows show a small drop for the highest flow rate, whereas the electricity consumption is the same. This brings a minor COP reduction for a flow rate of 1.35 m³/h of about 2-4 % compared to the other testing conditions.

Similar tests have been performed for a variable evaporator water flow rate in the range of 2.18 to 2.6 m³/h. This flow rate is higher than the one at the condenser, since the evaporator will be coupled with the hot side of the magnetocaloric heat pump, requiring a low water temperature difference. The test results for a variable evaporator flow rate are presented in Figs. 2.17-2.18.

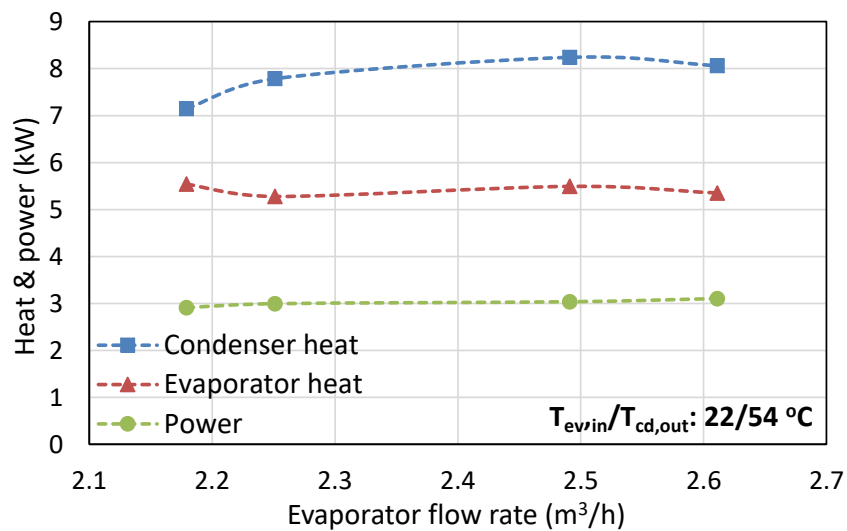


Fig. 2.17. Heat flows at the evaporator and condenser and electricity consumption of the heat pump for a variable evaporator water flow rate

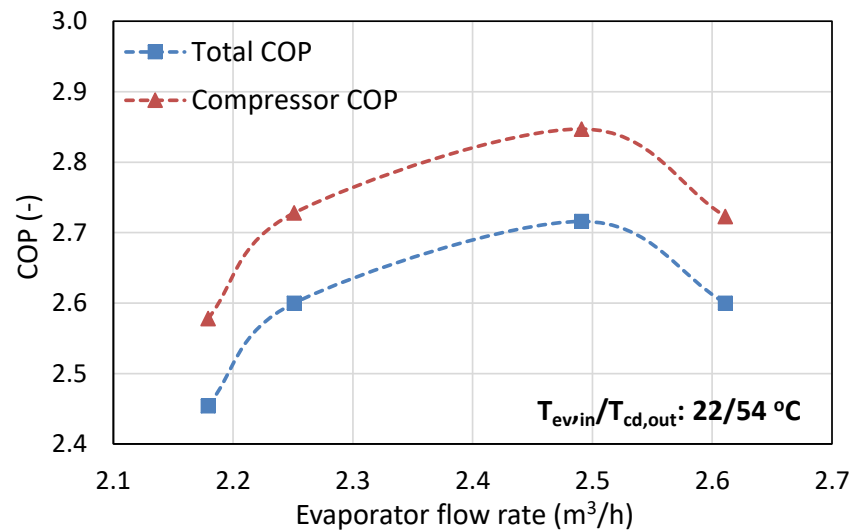


Fig. 2.18. Total and compressor COP of the heat pump for a variable evaporator water flow rate

The electricity consumption is again constant for all tests, but the heating capacity is increased for the moderate values of the flow rate. This has a direct positive impact to the COP since the pinch point temperature difference at the evaporator is reduced, leading to the increase of the evaporation pressure.

2.4 Conclusions and actions taken

The processing of the test results and the experience gained during the operation at NCSR D revealed that there is a large room for improving the heat pump performance. Such observations were supported by the calculated performance presented in D2.2. The most important one concerns the use of the same compressor type, but with a three-phase motor, which gives a higher efficiency by about 10-15% and comes with a much lower electrical current and inverter that greatly reduce the costs. This replacement has been accomplished by Psycrotherm as soon as the first tests at NCSR D were completed at the end of July 2020 and the unit was shipped back to their workshop. Other minor changes have been done as well, such as the addition of a better piping insulation at the hot parts of the cycle (refrigerant side, discharge and liquid lines) to reduce the heat losses. Once all these modifications had been accomplished, the heat pump was shipped to DTI for testing within a larger operating range.

3 Vapor compression heat pump testing at DTI

3.1 Test setup

The vapour compression heat pump was received at Danish Technological Institute (DTI), Aarhus, Denmark in September 2021. Afterwards, it was installed in a test setup in the laboratory that handles the characterisation of heat pumps.

The main purpose of the heat pump test at DTI was to perform an envelope test and to test the energy efficiency in different test scenarios under heating mode. Subsequently, these results would be compared to the test results from NCSR D.

The heat pump was charged with the prescribed 4 kg of the HFO refrigerant, R1234ze(E) and connected to temperature-controlled water flows on the evaporator and condenser side of the heat pump in closed circuits. Through heat exchange with external systems, the water circuit on the condenser was cooled and the water circuit on the evaporator side was heated in order to achieve the specified temperatures in the test scenarios. This was controlled by PID regulated valves with a given setpoint which either opened or closed depending on whether it was necessary to cool or heat. Same method applied for the control of the pumps and waterflow.

The outdoor air-fan evaporator was not part of these tests, with focus only on water-source mode.

The water flow for the evaporator and condenser was constant through the tests at 1400 and 2000 L/h. The cooling and heating of the water circuits were regulated to reach the specified water inlet and outlet temperatures from the heat pump at the evaporator and condenser, while the temperature differences between inlet and outlet was varying, depending on the effect of the heat pump.

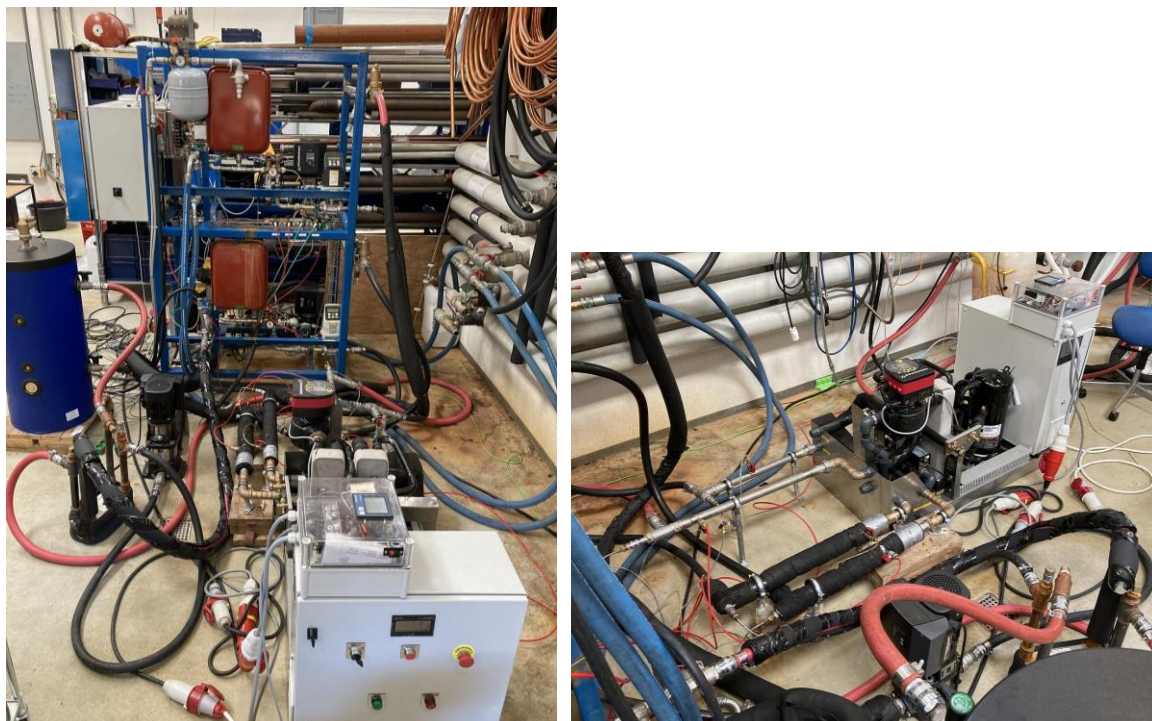


Fig. 3.1. Heat pump test setup at DTI

3.1.1 Stabilizing heat pump operation

When the heat pump was put into operation, the temperature on the water side of the condenser outlet showed large fluctuations, which meant that the heat pump was not operating optimally. Moreover, the sight glass showed bubbles in the refrigerant, which could be a sign of the lack of refrigerant in the refrigerant circuit of the heat pump.

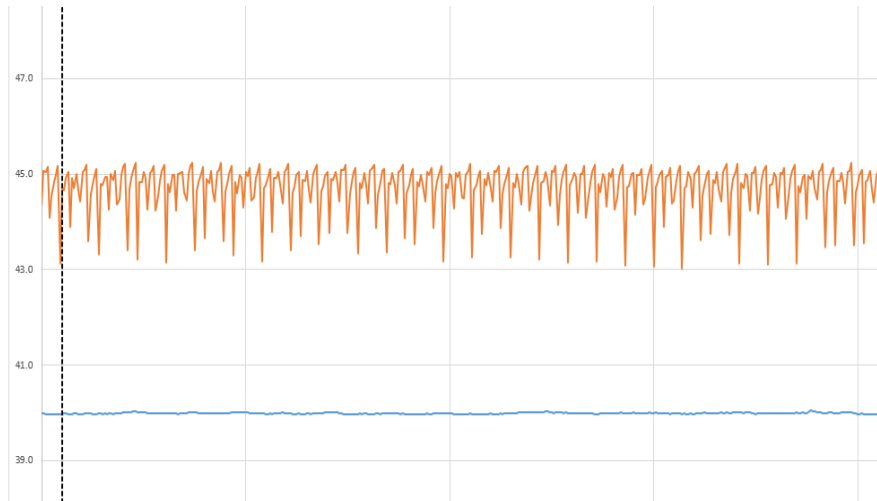


Fig. 3.2. Fluctuating temperatures in the condenser

Therefore, a process of troubleshooting took place in order to stabilize the operation. This included:

- Assessment of all heat pump settings, e.g. electronic expansion valve, thermostatic expansion valve for internal economizer, super heat regulation, etc.
- Emptying the refrigerant
- Replacement of thermostatic expansion valve at economizer
- Emptying the refrigerant and evacuating the heat pump
- Leakage detection with nitrogen
- Refrigerant refilling with 5.1 kg of HFO 1234ze(E)

After adding more refrigerant to the system, the fluctuations stopped and there were no more bubbles in the sight glass.

Moreover, the water temperature on the condenser side of the heat pump remained stable.

3.2 Test results

A test matrix was planned with varying temperatures at different compressor speeds and water flows.

The first test conditions are shown in the following matrix.

Table 3.1. Test Matrix 3a for the heat pump

| Evap. water inlet T | Condenser water outlet T | | | | |
|---------------------|--------------------------|----|----|----|----|
| | 35 | 40 | 45 | 50 | 55 |
| 5 | X | | X | | X |
| 10 | | | | | |
| 15 | X | | X | | X |
| 20 | | | | | |
| 25 | X | | X | | X |

The test results for the measured COP can be seen in the following table.

Table 3.2 COP results from heat pump test

| Evaporator water inlet Temp. [°C] | Condenser water outlet Temp. [°C] | | |
|--|--|-----------|-----------|
| | 35 | 45 | 55 |
| 5 | 2.21 | 1.17 | 0.93 |
| 15 | 3.73 | 2.66 | 1.63 |
| 25 | 5.17 | 4.09 | 3.07 |

The following figure shows the comparison of the COP test results from the tests at DTI and NRSCD.

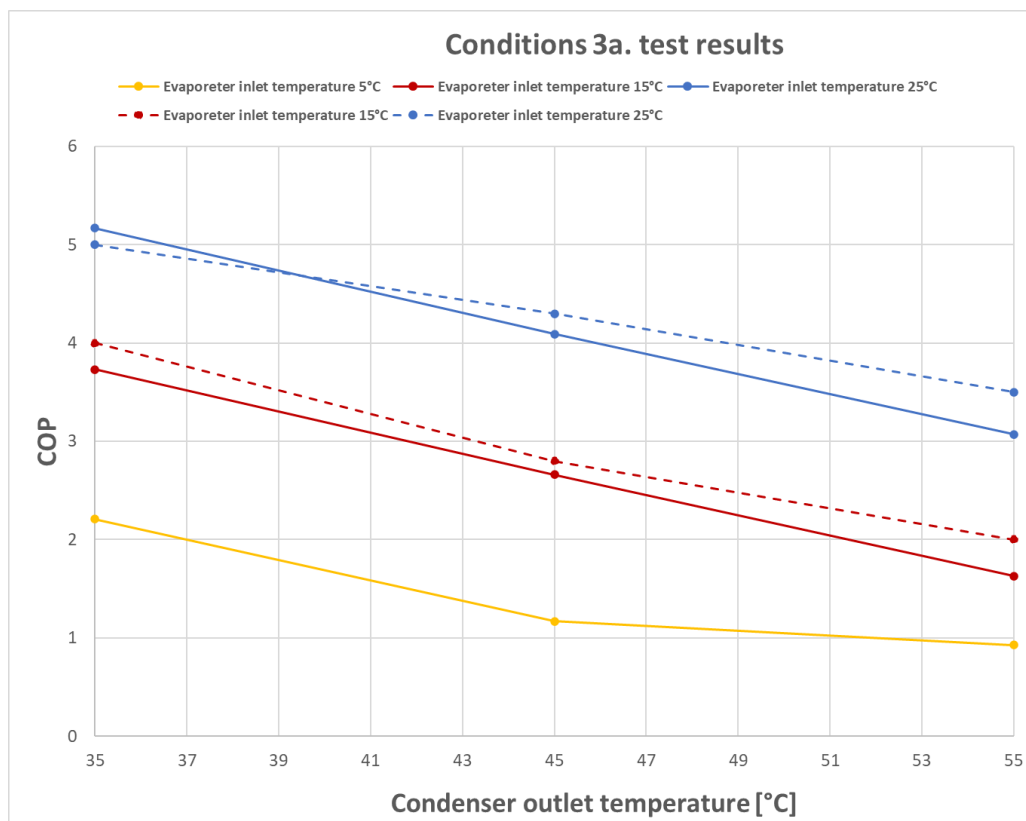


Fig. 3.3. COP test results from DTI compared to test results from NRSCD (dotted line)

The figure shows that the DTI results are 5-15% below the results from NRSCD, except the results from the 25/35°C test point.

3.2.1 Continuation of tests

Unfortunately, the DTI test results from the first test matrix did not show improved COP compared to the NRSCD test results, even if some modifications have been done. Further tuning of the economizer superheat could lead to a small improvement since some settings were not identical.

Moreover, the test results showed a Carnot efficiency of approximately 25 %, where the best vapour compression heat pumps on the market today can exceed 50% Carnot efficiency.

Therefore, it was decided not to perform the remaining test matrices with different compressor speeds and different water flows since other improvements will be implemented before the heat pump is included in the full pilot test carried out in work package 5 (see section 6).

4 The magnetocaloric heat pump in the integrated heat pump

4.1 Introduction

During operation of the magnetocaloric heat pump, the working fluid (i.e. water mixed with some corrosion inhibitor) is circulated by a centrifugal pump around the circuit and into the regenerator beds synchronized with the rotation of the magnet. The pump also connects the regenerator beds with the external heat exchangers (heat sink and heat source). On the cold side (connected to the heat source) of the magnetocaloric heat pump, there is an electric circulation heater, which is used to simulate a cooling load. The temperature of the cold fluid is measured before and after passing through the circulation heater, and the difference is used to establish the cooling power of the heat pump. On the hot side of the heat pump, there is a heat exchanger. One side is connected to the fluid loop of the heat pump, and the other is connected to a constant temperature bath (chiller), capable of extracting the heat at a constant temperature.



Fig. 4.1. Flow system of the magnetocaloric heat pump developed at DTU Energy

The parallel flow system comprises 13 hot-side outlet and 13 hot-side inlet solenoid valves, 26 check valves, 26 flow strainers with filters, and four manifolds. A simplified schematic of the fluid flow system of the heat pump is shown in Fig. 4.2.

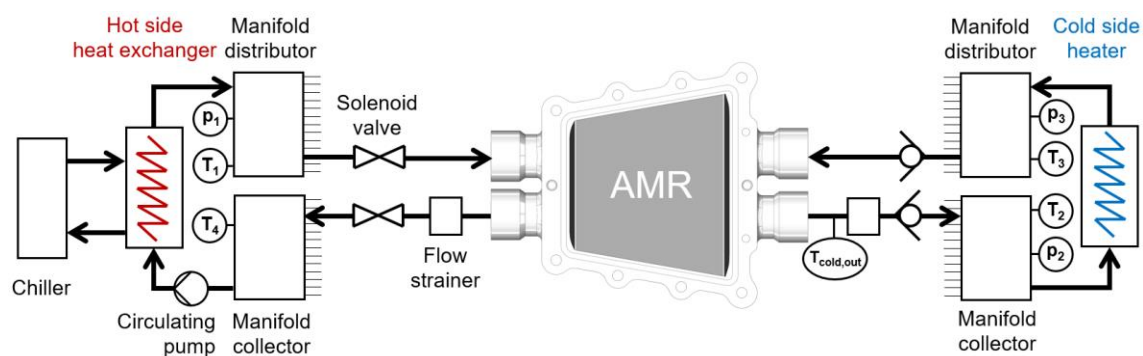


Fig. 4.2. Schematic view of the fluid flowing through one regenerator (AMR) bed

The heat pump needs to operate within the specific temperature range defined by the magnetocaloric material within the regenerator beds. The heat pump efficiency is quite sensitive to the temperature of the hot end, while the cold end temperature has more freedom in terms of variation, i.e. the temperature can vary several degrees without drastically affecting the heat pump performance.

Furthermore, the temperature difference between the outlet and the return fluid flow for both the hot and cold ends of the heat pump is quite small (less than 2 K). This must be taken into account when coupling the magnetocaloric heat pump to the vapour compression heat pump.

Table 4.1. Control parameters for operating the magnetocaloric heat pump

| Parameter | Range |
|----------------------------|---|
| Cycle frequency | 0.5 - 2 Hz |
| Volumetric fluid flow rate | 100 – 2000 L/hr |
| Valve opening behaviour | 'Start-up' mode 'Performance' mode 'Economy' mode |

The performance of the heat pump can be tested under various operating conditions (see Table 4.1). The first operating input parameter is the rotation frequency of the magnet assembly mounted on a shaft that is driven by the motor. The rotational frequency can go up to 2 Hz. The fluid flow rate can be regulated by controlling the pump velocity. The electromechanically operated solenoid valves allow a remotely control of the fluid flow through each regenerator synchronized with the magnetic field. The operation of the solenoid valves is position-controlled, meaning that an internal valve control algorithm monitors the magnet position via the encoder reading and opens/closes the solenoids at the appropriate time. Changing the opening and closing angle of each solenoid valve allows the individual control of the hot-to-cold and cold-to-hot blow into each regenerator bed. Depending on the application, different settings for the valve opening behaviour can be considered. For example, the setting 'Start-up' gives the fastest transient response at the hot and cold ends of the heat pump, and the heating load and coefficient of performance (COP) are not prioritized. 'Performance' settings provide the highest heating power at the expense of the COP, while 'Economy' settings give the best COP at a reduced maximum heating power.

4.2 Challenges in the testing of the magnetocaloric heat pump

The magnetocaloric heat pump has undergone a series of tests at DTU. The aim has been to test each heat pump component to ensure its functionality as well as to map out the performance under different operating conditions, such as cycle frequency, valve settings, and fluid flowrate. An extended test period (170 hours in total spread over multiple test series) was completed, resulting in a set of combinations of heating power, temperature span, and heat pump efficiency (in terms of COP and second-law efficiency). One of the initial tests yielded the following results: a heating power of 340 W and a COP of 6.7 at a temperature span of 11.6 K, a cycle frequency of 0.5 Hz, and a fixed hot end temperature of 295 K. Higher temperature spans can be reached, but at a lower heating power and efficiency. Varying the hot end temperature above or below 295 K, greatly reduced the heat pump performance. Further testing showed that modifying the valve control algorithm can improve the heat pump performance in terms of COP, but this is at the expense of a lower heating power. Increasing the cycle frequency can maximize the heating power of the magnetocaloric heat pump, but this yields lower efficiencies.

During multiple tests, it became apparent that the magnetocaloric heat pump is not yet fully stable for long-term operation. It requires much attention from experienced users in order to operate the heat pump. In addition, there have been issues, related to both the mechanical couplings, which affect the correct reading of the encoder angle, and the hydraulic system (i.e. check valves sticking open and clogged solenoid valves), which affect the desired fluid flow through the regenerator beds. Hence, the mechanical couplings and the components of the hydraulic systems needed modification,

replacement, or cleaning. Monitoring the functionality of these components before and during the running of the device is an important task for the operating personnel to ensure an efficient heat pump operation. Further challenges can be linked to the control of the heater at the cold end of the heat pump that made it difficult to accurately reach the desired cold end temperature or to achieve steady-state conditions. In addition, different operating conditions require different valve control algorithms, meaning that it is necessary to control the valves that result in an unbalanced flow through the regenerator bed. In order to obtain a balanced flow for all 13 beds, constant monitoring of the fluid temperature exiting the regenerator beds is required. Disassembling the heat pump for the move from DTU to DTI and the reassembly of it there would present a risk to the operation of it.

At the November 2020 GA meeting, it was decided that the magnetocaloric heat pump would not be shipped to DTI for the task 2.4 testing. Instead, testing of the magnetocaloric heat pump would continue at DTU throughout the following months. Meanwhile at DTI, the heat production will be simulated to represent the magnetocaloric heat pump.

4.3 Virtual integration of the magnetocaloric heat pump

4.3.1 Integration strategies

The integration of the two heat pump systems for heating production (i.e. the winter mode) would be in a cascade mode through the heat exchanger. This would allow different fluid types and flowrates on either side. This hydraulically disconnects the two heat pumps and allows for different temperature differences in the heat exchangers. In the absence of a borehole thermal energy storage (BTES) system, the magnetocaloric heat pump configured as the bottoming cycle of the integrated heat pump is supplied with low-temperature heat from PVT collectors via a solar buffer tank. However, large air temperature fluctuations during the heating season and a limited solar potential in winter are challenging for the magnetocaloric heat pump to operate within its optimal temperature range. Hence, it is preferred to use the vapour compression heat pump as the bottom cycle that supplies heat to the magnetocaloric heat pump, allowing the operation at its efficient temperature range to produce suitable space heating at a maximum temperature span. In the presence of a BTES system (or simulated BTES system), the most promising configuration of the integrated heat pump is the use of the magnetocaloric heat pump as the bottom cycle (providing heat to the evaporator of the vapour compression heat pump) as it can operate within its optimal temperature range, hence achieving better performance. The heat sink temperature to the vapour compression heat pump is constant, so the operation of the magnetocaloric heat pump can be controlled, e.g. by changing the operating frequency or valve setting mode. Another advantage is that this configuration can be used for both the heating and cooling modes. Hence, this is the desired configuration of the integrated heat pump test rig at DTI.

Due to the way the magnetocaloric effect works, a magnetocaloric heat pump will require certain conditions in order to operate optimally. One of these conditions is a fairly stable and fixed hot end temperature of around 20°C, depending on the operating conditions, whereas the cold end has more freedom. In principle, it may vary all the way from the design point around 2°C up to essentially the temperature of the hot end, giving a zero temperature span.

In addition, the fluid flow within the magnetocaloric heat pump is often very high, compared to the heat exchange circuit part of a vapor compression heat pump. For the heat exchanger connecting the two, this means that there may be a temperature difference of about 2 K on the magnetocaloric side, and a much larger difference on the vapour compression side.

4.3.2 Virtual integration

As the magnetocaloric heat pump was not moved to DTI, the connection between the two heat pumps was done virtually. In practice, this means that conforming experimental results from the two heat pumps are used together in a calculation of the overall performance. Thus, in practice, measurement series are chosen, where the hot end of the magnetocaloric heat pump matches the cold end of the vapour compression heat pump. In a physical coupling, a heat exchanger would be used to connect the two heat pumps. In the virtual coupling, this is done by the temperature match, assuming a highly efficient heat transfer in the heat exchanger. The heating power of the two heat pumps will not necessarily match up. In order to alleviate this, the power of the magnetocaloric heat pump was scaled to match that of the vapour compression heat pump, making sure to scale the input work as well. The power of the magnetocaloric heat pump scaling with the amount of magnetocaloric material in the heat pump is equivalent to simply building a larger heat pump.

5 Results for the integrated heat pump

The energy efficiency of the integrated heat pump will be calculated for a temperature increase of 50 K, corresponding to milestone MS6. Since it was not possible to combine the magnetocaloric heat pump and the vapour compression heat pump in the laboratory, virtual integration will be carried out instead.

5.1 Method for integration

The virtual integration uses the results achieved in the different laboratories, while considering the temperature levels needed for the serial coupling of the vapour compression heat pump and the magnetocaloric heat pump. The process is illustrated in Fig. 5.1.

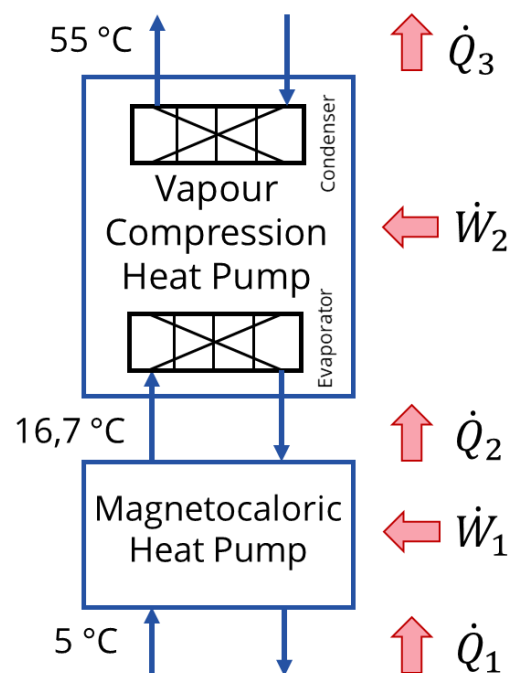


Fig. 5.1. Heat production and electricity consumption in the integrated heat pump

Where: $\dot{Q}_2 = \dot{Q}_1 + \dot{W}_1$ and $\dot{Q}_3 = \dot{Q}_2 + \dot{W}_2 \rightarrow \dot{Q}_3 = \dot{Q}_1 + \dot{W}_1 + \dot{W}_2$

The COP value can be calculated as: $COP = \frac{\dot{Q}_3}{\dot{W}_1 + \dot{W}_2}$

The two heat pumps have different capacities. In the calculation, this has not been considered since it is assumed the heat pump efficiencies of the different technologies can be rescaled in further developments.

The chosen temperature levels correspond to scenarios where the magnetocaloric heat pumps provide high COPs.

5.2 Evaluation of test results for the integrated heat pump

For the calculation of the overall COP for the integrated heat pump with a temperature increase of 50 K, the following test results are chosen:

Magnetocaloric heat pump: $T_{Cold} = 5^\circ\text{C}$, $T_{Warm} = 16.7^\circ\text{C}$, $COP = 6.7$

Vapour compression heat pump: $T_{Cold} = 16.7^\circ\text{C}$, $T_{Warm} = 55^\circ\text{C}$, $COP = 2.0$

The values of the vapour compression heat pump are from the heat pump test carried out at NCSR D. When looking at the COP values, it is important to take into account that the temperature increase of the vapour compression heat pump is much larger than the one for the magnetocaloric heat pump.

The calculated Carnot efficiencies (efficiency compared to the highest theoretical achievable value) of the two heat pumps are very similar with 27 % for the magnetocaloric heat pump and 25 % for the vapour compression heat pump.

The calculations show an overall COP of 1.75 for the integrated heat pump producing a temperature increase of 50 K from 5°C to 55°C.

When using the same values for the magnetocaloric heat pump, but calculating the overall COP with other temperature increases in the vapour compression heat pump, the following results are achieved.

Table 5.1. Calculated COPs for the integrated heat pump at different temperature increases

| Temperature span | Calculated overall COP based on test results | Calculated Carnot efficiency |
|------------------|--|------------------------------|
| 5°C - 55°C | 1.75 | 27 % |
| 5°C - 45°C | 2.26 | 28 % |
| 5°C - 35°C | 2.76 | 27 % |

However, calculations show that a COP of 4.5 would require an overall Carnot efficiency of 69 %. The best commercialized heat pumps on the market today have a Carnot efficiency just above 50 %. The milestone was therefore extremely ambitious and more difficult to achieve when including new innovative technologies.

The vapour compression heat pump did, however, not function in an optimal way, producing much lower efficiencies than expected.

If the same calculations are made with estimations on the vapour compression heat pump efficiency corresponding to the best available heat pumps on the market, the results are as follows:

Table 5.2. Calculated COPs for the integrated heat pump at different temperature increases with Carnot efficiencies for the vapour compression heat pump at app. 52%

| Temperature span | Calculated overall COP based on vapour compression heat pump market values | Calculated Carnot efficiency |
|------------------|--|------------------------------|
| 5°C - 55°C | 2.9 | 44 % |
| 5°C - 45°C | 3.3 | 42 % |
| 5°C - 35°C | 3.9 | 38 % |

The best vapour compression heat pumps available on the market will have a COP of approximately 3.5 at a temperature increase of 50 K.

6 Modifying the heat pump for enhancing the RES4BUILD system performance

6.1 Evaluation of heat pump test results and necessary modifications

6.1.1 Evaluation of test results and compressor efficiency

Although improvements have been done by Psycrotherm before the vapour compression heat pump was shipped to DTI, the performance was still lower than expected as is revealed from the previous sections. The main reason for this is the under-performing scroll compressor, which is originally provided for operation with the refrigerants R407C (with vapour injection) and R134a (without vapour injection). Both refrigerants operate at higher pressures than the selected R1234ze(E), which has been considered as a positive aspect in the initial development stages since the mechanical and friction losses of the compressor were expected to be lower. However, this turned up to be the main shortcoming, leading to a low isentropic efficiency after processing the measured data. This efficiency is shown in Fig. 6.1 as a function of the pressure ratio (top) and pressure difference (bottom). The red curves show the expected efficiency, which is slightly lower than the performance with R407C as reported by the compressor manufacturer.

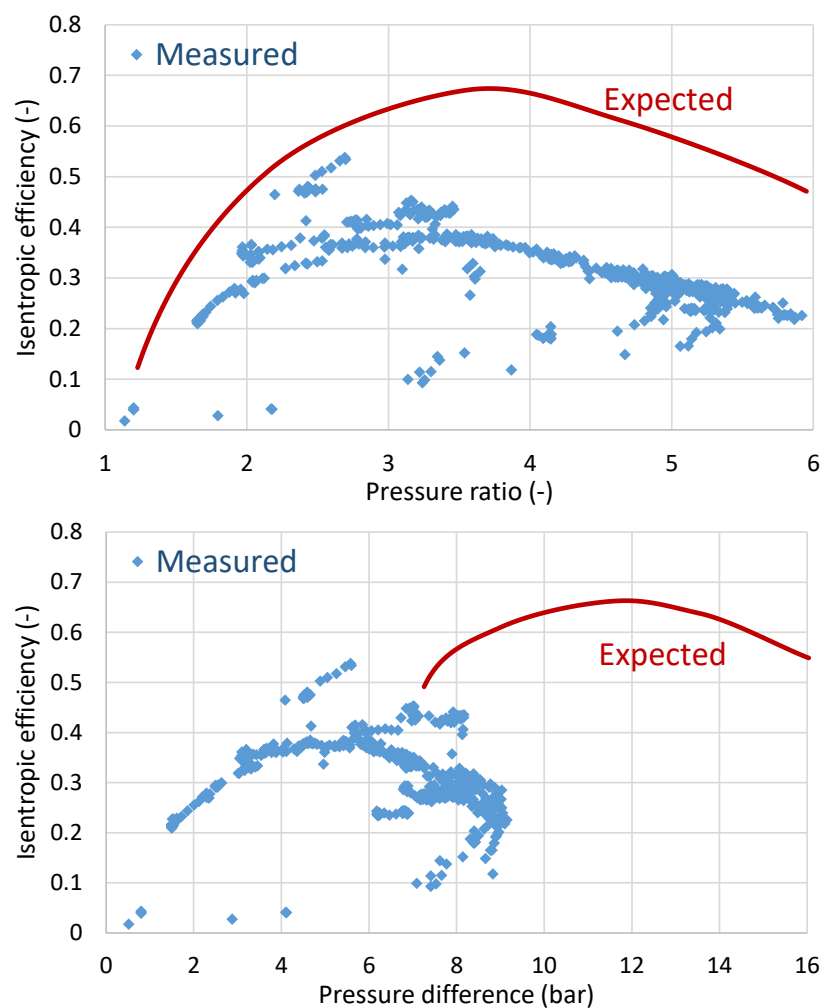


Fig. 6.1. Measured and expected isentropic efficiency of the compressor with R1234ze(E) as a function of pressure ratio (top) and pressure difference (bottom)

The measured pressure ratio is within the range of the compressor's envelope, but the suction and discharge pressures are lower by about 4 and 8 bar, respectively. This brings a much lower pressure difference with a low suction density as shown in the second graph. This is the main reason why the maximum isentropic efficiency is reduced by about 35 % (from almost 70 % to just 45 %), bringing a negative impact to the COP (measured even two times lower COP values compared to the expected values), especially at low heat source temperatures (low suction pressure) as presented in the previous sections.

It should be mentioned here that all other parts of the heat pump operated very well; the heat exchangers show a low pinch point temperature difference between the refrigerant flow and the water, and the electronic expansion valve keeps an almost constant superheat. Therefore, special focus has been given to the compressor in order to understand the magnitude of the main losses.

For this purpose, a semi-empirical model has been adjusted by NCSR D based on a well-established methodology² and extended for vapour injection compressors³. The performance indicators (e.g. isentropic and volumetric efficiency) have been defined based on recent practices⁴. According to this approach, the entire compression process has been divided into several steps, as depicted in Fig. 6.2, without considering the lubricating oil flow. The processes included in the compressor modeling are explained next:

1. Supply (adiabatic) pressure drop at the suction port and the motor (1→2)
2. Isobaric heating-up due to the hot motor and the casing, which are maintained at a higher average temperature than the refrigerant at the suction (2→3)
3. Mixing of supply flow with the leakage flow, with the latter undergoing a throttling process which reduces its pressure (6+3→4)
4. First isentropic compression of the refrigerant to the intermediate pressure (4→5)
5. Adiabatic mixing of the compressed refrigerant with the vapour injection at the intermediate pressure (5+5a→5b)
6. Second isentropic compression of the refrigerant (5b→5c)
7. Adiabatic compression at constant volume (5c→6)
8. Leaking flow to the compressor inlet
9. Exhaust isobaric cooling due to the lower temperature of the fictitious isothermal wall than that of the exhaust refrigerant (6→7)
10. Pressure drop at the exhaust port reaching the discharge pressure (7→8).

² Winandy E, Saavedra C, Lebrun J. Experimental analysis and simplified modelling of a hermetic scroll refrigeration compressor. *Applied Thermal Engineering* 2002;22(2):107-20.

³ Dardenne L, Fraccari E, Maggioni A, Molinaroli L, Proserpio L, Winandy E. Semi-empirical modelling of a variable speed scroll compressor with vapour injection. *International Journal of Refrigeration* 2015;54:76-87.

⁴ Tello-Oquendo FM, Navarro-Peris E, Barceló-Ruescas F, González-Maciá J. Semi-empirical model of scroll compressors and its extension to describe vapor-injection compressors. Model description and experimental validation. *International Journal of Refrigeration* 2019;106:308-26.

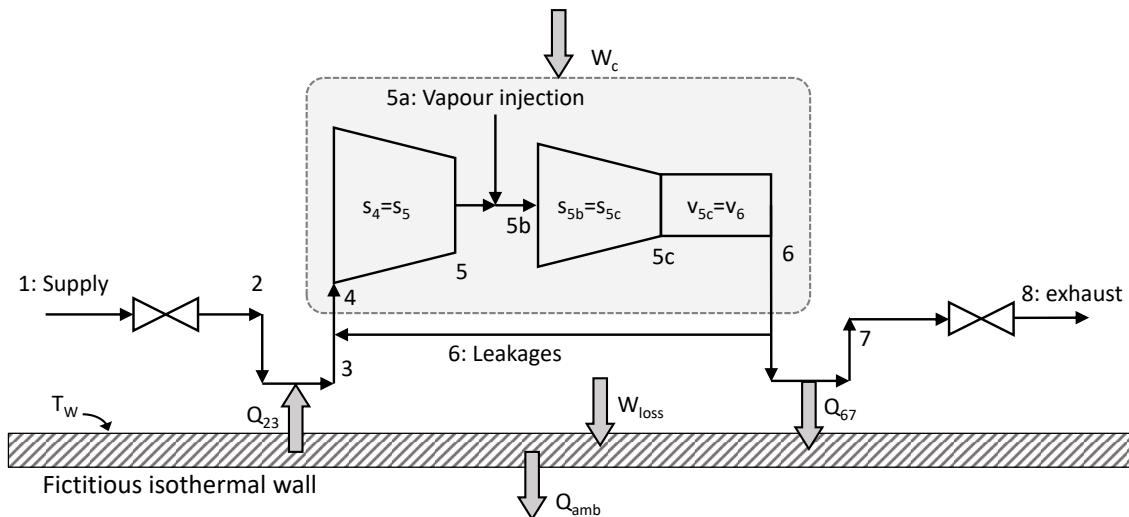


Fig. 6.2. Compressor processes of the semi-empirical approach

A part of the measured data under water-source operation covering the whole range of heat source and sink temperatures has been used for the model calibration in order to calculate the values of the six parameters below. This calculation has been performed by means of an optimisation method with genetic algorithms for minimizing the relative difference of discharge temperature, electricity consumption, and refrigerant mass flow rate under the Engineering Equation Solver (EES) environment⁵. The values of the calibrated parameters and the related sub-processes of the compression are presented in Table 6.1.

Table 6.1. Parameters of the semi-empirical model and relevant compressor sub-processes

| Parameter | Value | Units | Sub-process |
|--------------|----------------------|-------|---|
| AU_{su} | 1.236 | W/K | Refrigerant heating-up during supply |
| AU_{dis} | 334.6 | W/K | Refrigerant heat loss during exhaust |
| AU_{amb} | 1287 | W/K | Heat losses to the ambient |
| A_{leak} | $1.77 \cdot 10^{-6}$ | m^2 | Effective area of leakages |
| $W_{loss,0}$ | 616.8 | W | Constant term of the electric losses |
| α_c | 0.414 | - | Coefficient of the variable term of the electric losses |

This model is able to predict the compressor discharge temperature, the refrigerant flow rate, the ambient losses, and the compressor electrical power by using the condensing and evaporating pressures, supply temperature, surrounding temperature, and compressor speed as well as displacement as inputs. The results of this process are shown in Figs. 6.3-6.5 which show the comparison of the calculated and the measured values. The refrigerant mass flow rate is not directly measured, but it is calculated from the energy balance of the evaporator based on the measured inlet/outlet temperatures of the water and the refrigerant and the measured water flow rate. The same approach is followed in terms of the condenser in order to calculate the mass flow rate of the vapour injection flow to the compressor.

⁵ Klein SA. Engineering Equation Solver-EES (64-bit), version 10.834. Academic Professional; 2020. <http://www.fchartsoftware.com/ees/>.

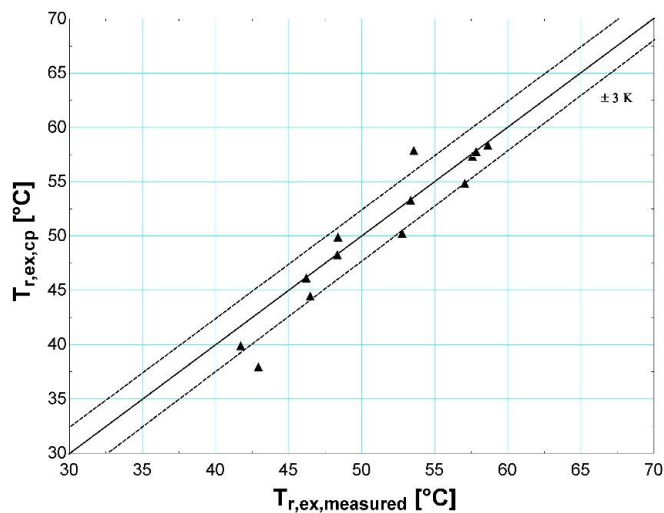


Fig. 6.3. Comparison of the calculated and measured discharge temperature

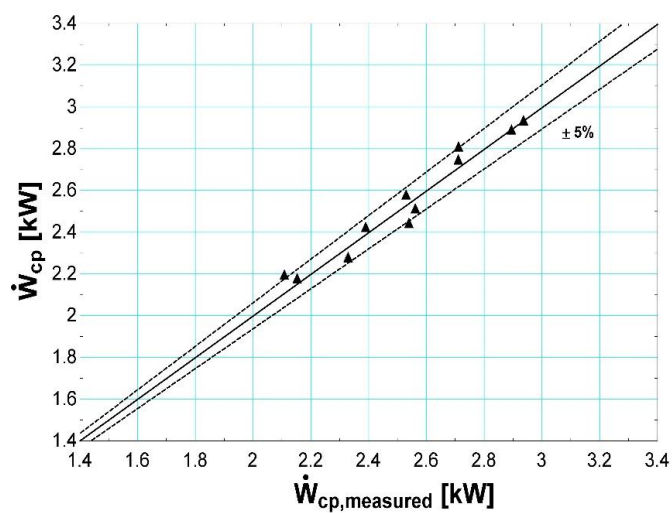


Fig. 6.4. Comparison of the calculated and measured power of the compressor

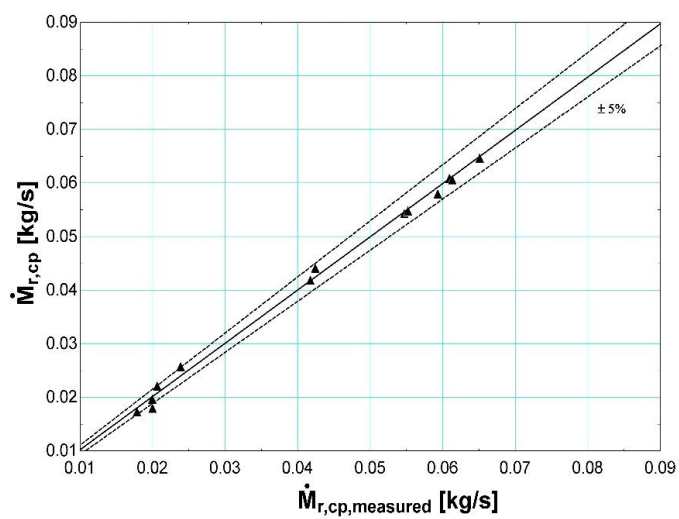


Fig. 6.5. Comparison of the calculated and measured refrigerant mass flow rate

The model predicts the mass flow rate and the electricity consumption with a very good accuracy, all calculated values within $\pm 5\%$. The discharge temperature is predicted in most of the cases within a range of $\pm 3\text{ K}$ of the measured value.

This methodology provides insights of the energy losses within the compressor unit (e.g. pressure, heat, and electrical losses) and it has been proved to be extremely helpful for the current case, with the aim to better understand the losses mechanism in the selected compressor that is developed for other refrigerants (high-GWP refrigerants) from the one used here (low-GWP).

The loss that is responsible for the largest reduction of the compressor performance and subsequently of the whole heat pump cycle is the suction pressure drop. The main reason for this is the low suction density compared to the one that the scroll compressor is designed for (about 2-3 times lower). This drop even reaches 1.5 bar, as shown in Fig. 6.6 as a function of the pressure ratio. This is very high considering that the highest suction pressure is about 3.5 bar.

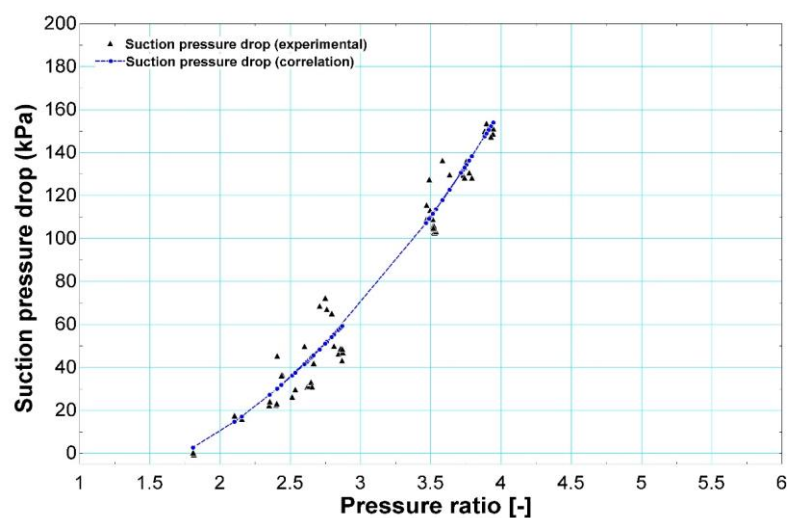


Fig. 6.6. Suction pressure drop as a function of the pressure ratio

In order to better evaluate the effect of the suction pressure drop on the compressor performance, additional simulation runs have been conducted with the use of the calibrated semi-empirical model, but with an artificially reduced suction pressure drop. This kind of calculations are helpful as to identify the compressor power and efficiency. The results of the isentropic efficiency, the volumetric efficiency, and the power consumption for different levels of the suction pressure drop (from 50 to 200% less, denoted as “ $dP_{suction}/1.5$ ” etc.) are shown in Figs. 6.7-6.9, respectively.

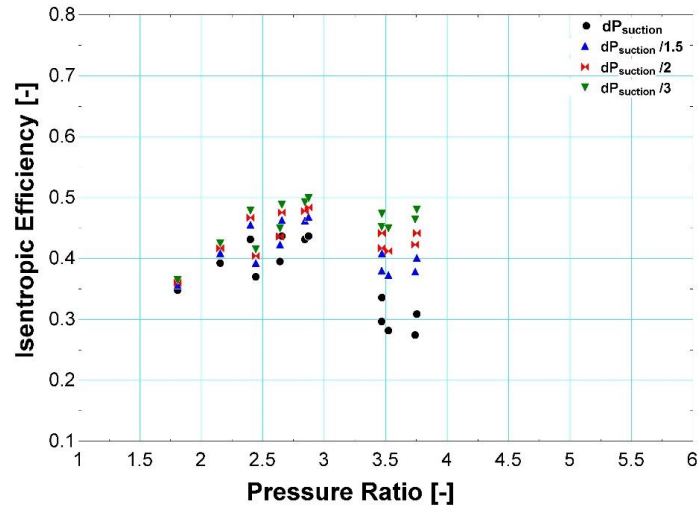


Fig. 6.7. Compressor isentropic efficiency for various levels of suction pressure drop

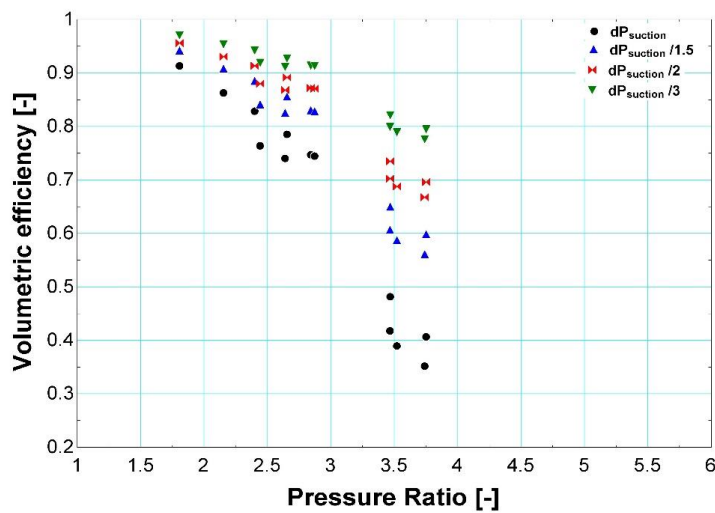


Fig. 6.8. Compressor volumetric efficiency for various levels of suction pressure drop

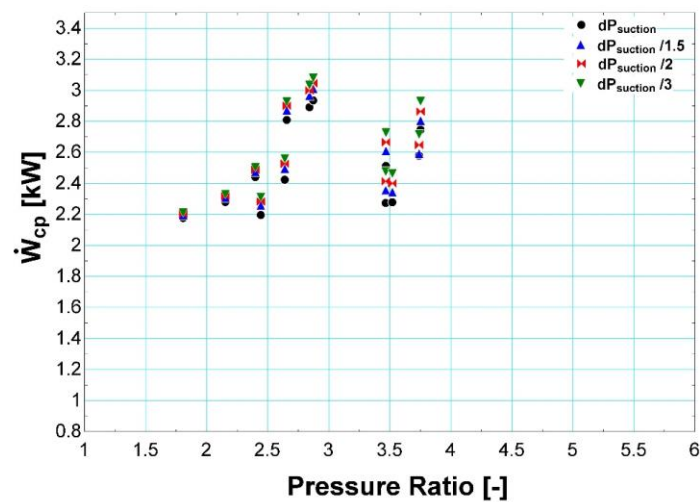


Fig. 6.9. Compressor power consumption for various levels of suction pressure drop

The electricity consumption of the compressor shows a small variation when the suction pressure drop is reduced, but the isentropic and volumetric efficiency are greatly improved since a much higher refrigerant mass flow rate enters the compressor. This leads to an increase of the condenser heat and subsequently of the COP as well a double increase of a high-pressure ratio.

6.1.2 Modifications for increasing the performance

Once the heat pump tests at DTI had finished and all the results were evaluated, it was decided to replace the compressor and the refrigerant in order to improve the performance of the heat pump and to approach the performance of high-efficiency commercial products based on HFC refrigerants (e.g. R407C, R410a, R134a). In order to do so, the heat pump was shipped back from DTI to Psycrotherm in May 2021 for the handling of these modifications.

An evaluation of available compressors has been initiated, mostly focusing on a new series of scroll compressors by Copeland, the YH series, which is suitable for HFO blends⁶ and has been released since the beginning of 2021. Another suitable series is the Copeland ZR one for different HFO blends. A comparative analysis of the different combinations of compressors and refrigerants has been performed, based on the calculations of the Copeland selection software with a typical suction superheat of 5 K and a subcooling of 2 K. This has been done for compressors with a maximum heating capacity of about 10 kW, matching the needs of the pilot system.

The key result concerns the COP for heating, which is shown in Fig. 6.10 for different evaporation and condensation temperatures. The 15/45°C and 15/55°C cases correspond to the heating supply from the magnetocaloric heat pump (supply temperature in the range of 20-25°C) for heat production of space heating and hot water, respectively, whereas the 0/55°C case corresponds to the by-passing of the magnetocaloric heat pump with the heat source from the BTES directly supplying the vapour compression heat pump. In the same graph, the COP of the heat pump is also highlighted with the ZH13 compressor with vapour injection using the refrigerant R407C, which is the same compressor that has been used during the tests, but with another refrigerant (R1234ze(E)).

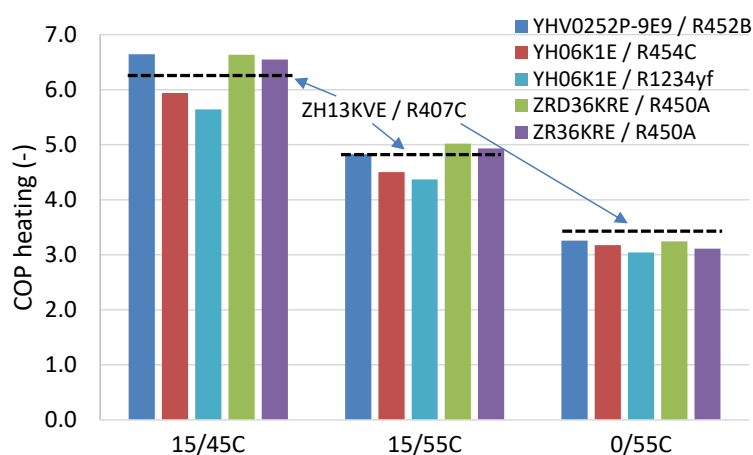


Fig. 6.10. COP for heating of different pairs of compressors and refrigerants for representative evaporation and condensation temperatures

⁶ Copeland scroll compressor YH series: <https://climate.emerson.com/en-gb/shop/1/climate-technologies/copeland-eu-copeland-scroll-yh1e-compressors-en-gb?fetchFacets=true#facet:&partsFacet:&facetLimit:&productBeginIndex:0&partsBeginIndex:0&orderBy:&partsOrderBy:&pageView:&minPrice:&maxPrice:&pageSize:&>

The ZR compressor with R450A brings the highest performance at all conditions and would be the favoured choice. However, the refrigerant R450A has a GWP of 650, which is about the half compared to standard refrigerants, but it will probably face future restrictions according to the F-Gas regulation⁷ since its GWP is over 150. Only one of the refrigerants shown in the previous graph meets this restriction, R454C, as its GWP is 148, as shown in Table 6.2.

Table 6.2. GWP and ASHRAE class of the candidate refrigerants

| Refrigerant | Type | GWP | ASHRAE class |
|-------------|-----------|-----|--------------|
| R452B | HFO blend | 698 | A2L |
| R1234yf | HFO | 4 | A2L |
| R454C | HFO blend | 148 | A2L |
| R450A | HFO blend | 650 | A1 |

Although the COP with R454C is about 10 % lower than the others, it has been selected for the heat pump due to its very low GWP. The same compressor with R1234yf (a pure HFO with an ultra-low GWP) has an even lower COP, about 5-10 % lower. For that purpose, the YH06 compressor with R454C has been decided to replace the previous compressor, with the necessary work conducted by Psycrotherm during the summer of 2021. Tests will then be carried out by both Psycrotherm in Greece and DTI in Denmark to verify the performance. This activity belongs to Task 5.3 and is presented in deliverable D5.3.

6.1.3 Numerical model of the improved heat pump

According to the performance indicators provided by the compressor manufacturer, an equation-fitting procedure has been conducted in order to produce a suitable model to be used in the system simulations, using the numerical tools developed in Task 3.1. By considering a reasonable pinch point temperature difference at the evaporator and condenser, a typical suction and discharge pressure drop (each corresponding to 0.2 K temperature drop), a subcooling of 2 K, and a useful superheat of 7 K, performance maps have been produced as a function of water and air temperatures for water-source and air-source operation, respectively. The resulting COP is presented in Fig. 6.11 for heating (left) and cooling (right) with water, while Fig. 6.12 shows the similar graphs, but with air.

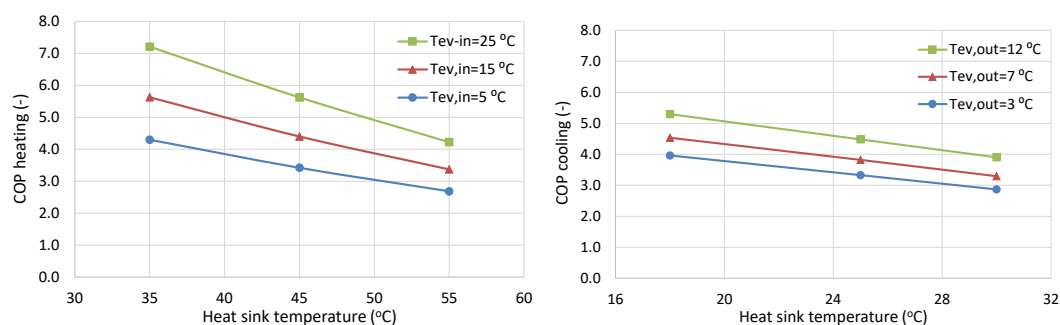


Fig. 6.11. COP of the YH06 compressor with R454C for different heat sink and source temperatures for heating (left) and cooling (right) with water

⁷ F-Gas regulation / Regulation (EU) No 517/2014 of the European Parliament and of the Council of 16 April 2014 on fluorinated greenhouse gases and repealing Regulation (EC) No 842/2006 Text with EEA relevance: <https://eur-lex.europa.eu/eli/reg/2014/517/oj>.

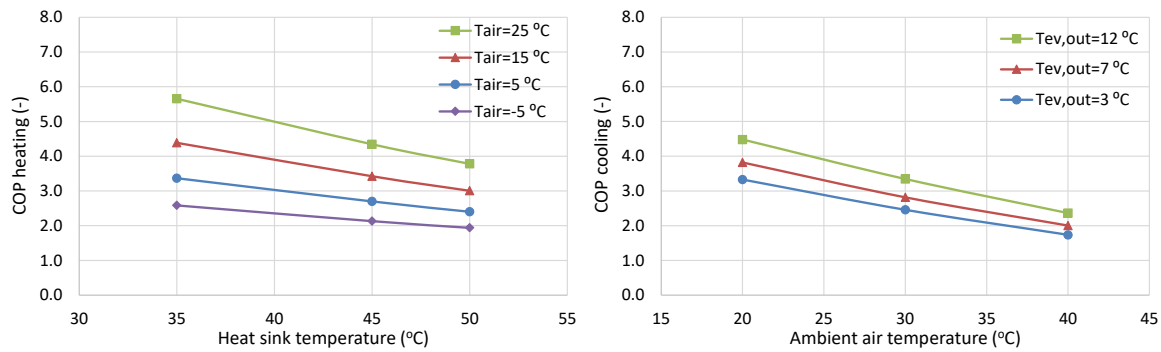


Fig. 6.12. COP of the YH06 compressor with R454C for different heat sink and source temperatures for heating (left) and cooling (right) with air

A fitting procedure followed in order to produce suitable correlations. The heat flows at the evaporator and condenser, the electricity consumption, and the COP have been included in the regression analysis, producing 2nd-order polynomial equations as a function of the sink and source temperatures with a R^2 of over 99.5 %.

These correlations of the heating capacity and the COP for heating are given by Eqs. (6.1)-(6.4) as a function of the outlet water temperature at the condenser and the inlet temperature at the evaporator (either water or air). The range of validity is:

- Outlet water temperature from the condenser ($T_{cd,out}$): 35–55 °C
- Inlet water temperature to the evaporator ($T_{ev,in}$): 5–25 °C
- Inlet ambient air temperature to the evaporator ($T_{air,in}$): -5–25 °C

Heating / water-source

$$Q_{cd} = 6.89972222E + 00 + 3.018333E - 01 T_{ev,in} + 4.316667E - 03 T_{ev,in}^2 - 3.81666667E - 02 T_{cd,out} + 2.166667E - 04 T_{cd,out}^2 - 3.3000E - 03 T_{ev,in} T_{cd,out} \quad (6.1)$$

$$COP_h = \frac{Q_{cd}}{P_e} = 7.56888889E + 00 + 2.32583333E - 01 T_{ev,in} + 1.11666667E - 03 T_{ev,in}^2 - 1.40583333E - 01 T_{cd,out} + 8.666667E - 04 T_{cd,out}^2 - 3.450E - 03 T_{ev,in} T_{cd,out} \quad (6.2)$$

Heating / air-source

$$Q_{cd} = 5.47288690E + 00 + 2.41023810E - 01 T_{air,in} + 3.241667E - 03 T_{air,in}^2 - 1.99214286E - 02 T_{cd,out} + 5.00E - 05 T_{cd,out}^2 - 2.43285714E - 03 T_{air,in} T_{cd,out} \quad (6.3)$$

$$COP_h = \frac{Q_{cd}}{P_e} = 6.170250E + 00 + 1.7960E - 01 T_{air,in} + 9.500E - 04 T_{air,in}^2 - 1.18733333E - 01 T_{cd,out} + 7.66667E - 04 T_{cd,out}^2 - 2.7600E - 03 T_{air,in} T_{cd,out} \quad (6.4)$$

The produced correlations of the evaporator heat (i.e. the cooling delivery) and the COP for cooling are given by Eqs. (6.5)-(6.8) as a function of the outlet water temperature at the evaporator and the water inlet temperature at the condenser (with water) or inlet ambient air temperature (with air). The range of validity is:

- Inlet water temperature to the condenser ($T_{cd,in}$): 18-30 °C
- Outlet water temperature from the evaporator ($T_{ev,out}$): 3-12 °C
- Inlet ambient air temperature to the condenser ($T_{air,in}$): 20-40 °C

Cooling / water sink

$$Q_{ev} = 5.61610907E + 00 + 2.53178729E - 01 T_{ev,out} + 4.01851852E - 03 T_{ev,out}^2 - 4.00927625E - 02 T_{cd,in} - 2.222E - 04 T_{cd,in}^2 - 2.77522936E - 03 T_{ev,out} T_{cd,in} \quad (6.5)$$

$$COP_c = \frac{Q_{ev}}{P_e} = 4.99562905E + 00 + 1.81476510E - 01 T_{ev,out} + 1.24074074E - 03 T_{ev,out}^2 - 7.75448773E - 02 T_{cd,in} - 1.1111E - 04 T_{cd,in}^2 - 2.8650925E - 03 T_{ev,out} T_{cd,in} \quad (6.6)$$

Cooling / air sink

$$Q_{ev} = 5.32370856E + 00 + 2.50654220E - 01 T_{ev,out} + 3.53703704E - 03 T_{ev,out}^2 - 3.83606557E - 02 T_{air,in} - 2.6667E - 04 T_{air,in}^2 - 2.95081967E - 03 T_{ev,out} T_{air,in} \quad (6.7)$$

$$COP_c = \frac{Q_{ev}}{P_e} = 5.02727687E + 00 + 1.68864602E - 01 T_{ev,out} + 1.20370370E - 03 T_{ev,out}^2 - 1.17557377E - 01 T_{air,in} + 7.833E - 04 T_{air,in}^2 - 2.94672131E - 03 T_{ev,out} * T_{air,in} \quad (6.8)$$

The above correlations are used in the system simulations to describe the operation and performance of the heat pump unit.

6.2 RES4BUILD system performance

The system performance including the heat pump is examined by means of the simulation tools developed by NCSRD in Task 3.1. The considered system layout is presented next, together with the heating and cooling demand.

6.2.1 System overview and operating modes

The integrated system includes the PVT collectors for producing heat and electricity and the multi-source heat pump for heating and cooling, once coupled with a BTES field. The system is intended to cover the space heating/cooling and DHW demand of a multi-family residential building (reference building). The heating and cooling modes are illustrated in Fig. 6.13, along with the main system components and their connections and the possible heat source and sink options.

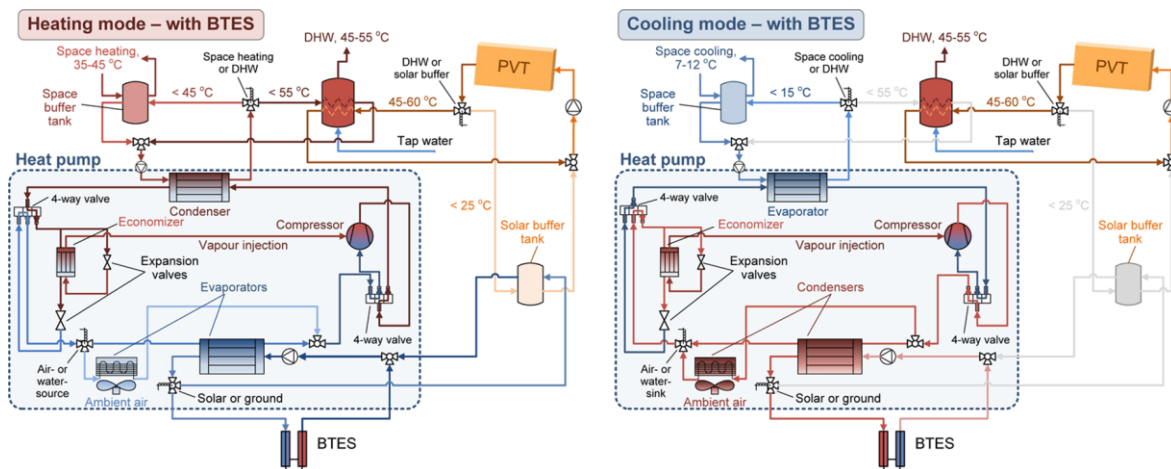


Fig. 6.13. System layout with the PVT collectors, the multi-source heat pump, the BTES, and the three water tanks. Left: Heating mode, Right: Cooling mode

Heating mode

At moments with high solar irradiation, the heat produced by the PVT collectors charges the main water tank that is used for covering the DHW needs of the building. Otherwise, when the solar radiation is low, the produced heat is stored in another tank (the so-called “solar buffer tank”), which is kept at a lower temperature and used as a heat source to the evaporator of the heat pump, which then charges the main tank for DHW up to 55 °C or the space buffer tank for space heating up to 45 °C. The latter stores heat that is supplied to the building to cover the demand for space heating, and it enhances the system flexibility, by decoupling to some extent the time of heating demand with the heat pump operation, with an overall aim of reducing the electricity demand from the grid.

There are three options for the heat source of the heat pump, selecting the one that maximizes the COP: (1) water-source from the BTES, (2) water-source from the solar buffer tank, and (3) air-source from the ambient. The most efficient is to operate at water-source mode, with the selection based on the highest temperature of either the BTES or the solar buffer tank. The air-source is only selected, when the ambient temperature is higher than about 7 °C of the water temperature, which takes place only during the summer season for DHW production.

Cooling mode

During the cooling mode in the summer season, the space buffer tank is charged with cold water at a minimum temperature of about 7 °C for delivering space cooling to the building. This is accomplished by reversing the heat pump operation with the use of two 4-way valves, while no simultaneous production of DHW and space cooling is possible, always giving priority to the DHW. Options similar to heating mode apply to the selection of the heat sink of the heat pump for rejecting heat to: (1) the BTES, or (2) the ambient air.

6.2.2 Heating and cooling demand

The multi-family residential building that serves as the case study has a total surface of 500 m² (five floors/apartments of 100 m² each). Two locations are considered: Athens (Greece) and Copenhagen (Denmark). The building requires hot water (DHW) all year round as well as space heating and cooling according to the season.

6.2.2.1 DHW demand

The DHW demand required by the model is calculated according to the EN16147:2017 standard for water-heaters, hot water storage appliances, and water heating systems⁸. The standard defines a 24-hour measurement tapping cycle with a draw temperature and flow rate leading to the calculation of the total thermal energy of 11,655 kWh per apartment/per day, corresponding to the “L” profile. Instead of using the same profile every day and for every location, an adjusted profile has been developed based on the thermal energy defined by the above standard. The annual temperature variation of the tap water in each location and the seasonal variability in hot water have been introduced⁹, while positively or negatively shifting the profile of each apartment by 15 minutes, in

⁸ Directive 2009/125/EC of the European Parliament and of the Council with regard to ecodesign requirements for water heaters and hot water storage tanks, EU Regulation No 814/2013 2 August 2013: <https://eur-lex.europa.eu/eli/reg/2013/814/2017-01-09>.

⁹ D’ Antoni M, Fedrizzi R, Sparber W, Haller M, Solartechnik S, IEA-SHC Task 44 / HPP Annex 38, 2013.

order to avoid overlapping all DHW demands at the same time. The monthly DHW demands of the buildings at both locations are presented in Fig. 6.14.

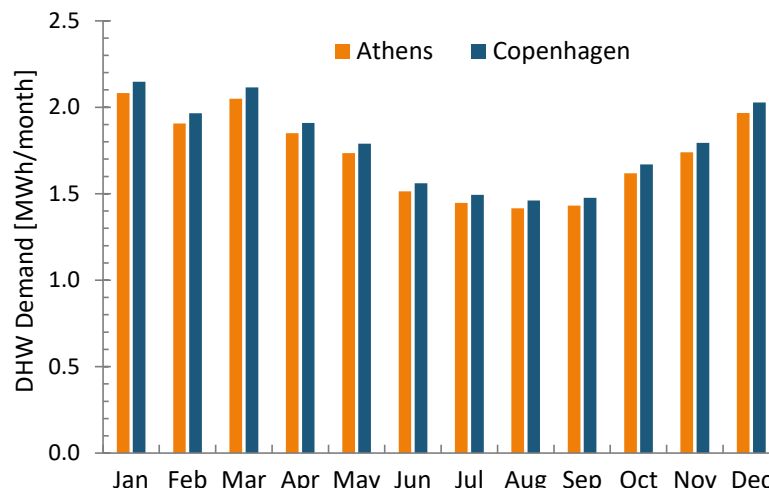


Fig. 6.14. Monthly DHW demand of the 5-apartment building in Athens and Copenhagen

6.2.2.2 Space heating/cooling demand

The space heating/cooling demand profile is estimated by an in-house Python code developed by NCSR D exclusively for this purpose. The numerical methodology is based on thermal zones (one for each floor, for multi-family residential buildings), thermostat preferences, building specifications (e.g. surface area and U-values of the walls), solar heat gains, and internal gains from occupants¹⁰. A smart thermostat approach is introduced into the code to restrict the sharp increase of space heating and cooling demand at peak hours, and thus smooth the profiles, indicating a realistic handling of the building loads. Furthermore, it is considered that the temperature on each floor is stabilized to a certain value when occupants are absent, based on typical occupancy profiles. Calculation of the necessary thermal loads to keep the indoor air temperature to the set-point temperature, allowing a variation of ± 1 K, is based on the distinction between heating and cooling seasons¹¹.

The U-values of the walls, roof, and windows have been adjusted for a 20-year old building, according to the Tabula database¹². The cumulative monthly space heating/cooling demands for the 5-apartment buildings in Athens and Copenhagen are shown in Fig. 6.15. It should be noted that due to the local weather conditions and the thermostat set-point for cooling at 26 °C, there is no need for cooling in Copenhagen.

¹⁰ Hoogsteen G., Molderink A., Hurink J.L., Smit G.J.M., Generation of flexible domestic load profiles to evaluate Demand Side Management approaches. In: 2016 IEEE Int. Energy Conf. ENERGYCON 2016, Institute of Electrical and Electronics Engineers Inc., 2016 April 4-8; Leuven, Belgium.

¹¹ Meramveliotakis G, Kosmadakis G, Krikas A, Gomes J, Pilou M. Innovative Coupling of PVT Collectors with Electric-Driven Heat Pumps for Sustainable Buildings. In: EuroSun 2020 - 13th Int. Conf. Sol. Energy Build. Ind., 2020 Sep 1-3; Athens, Greece.

¹² TABULA WebTool 2013: <https://webtool.building-typology.eu>.

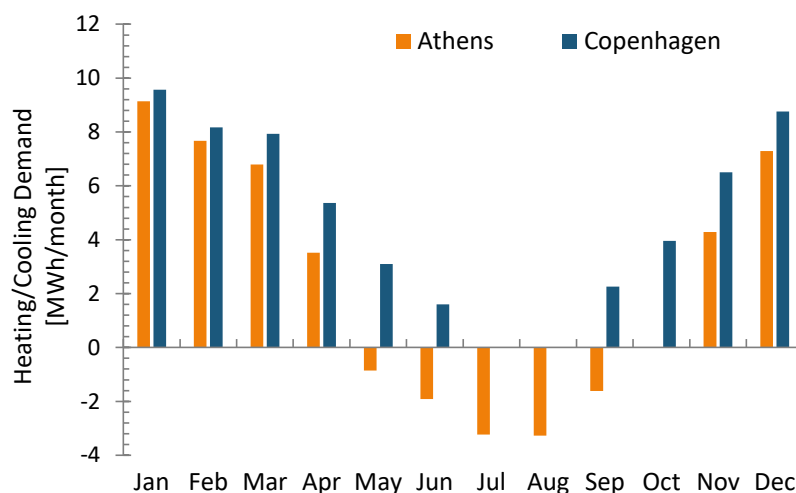


Fig. 6.15. Monthly space heating and cooling demands of the 5-apartment buildings in Athens and Copenhagen

6.2.3 Parameters and cases examined

The necessary weather data to perform the calculations have been obtained from Trnsys software, using the Type 109 component of this software, which reads the available TMY2 weather data for the defined 15-minute time-step. The processed data includes the solar radiation components on a tilted surface and the angle of incidence with a fixed tilt of 30° and an azimuth of 0° . For the simulations presented here, the TMY2 weather data for Athens and Copenhagen has been used to extract the necessary solar irradiation components (beam, diffuse, and total) as well as the ambient temperature during the whole year.

The total surface of the PVT collectors is 75 m^2 , and the volumes of the tanks are 2 m^3 for the DHW tank, 1.5 m^3 for the solar buffer tank, and 3 m^3 for the space buffer tank. This tank sizing corresponds to a specific volume of about 50 lt/m^2 , being a typical value for solar thermal applications.

The boreholes of the BTES field have a depth of 80 m and the mean surface temperature is 18°C in Athens and 9.4°C in Copenhagen, whereas the amplitude of the surface temperature is 7.2°C in Athens, and 8.9°C in Copenhagen. These values have been resulted from weather data processing from PVGIS tool¹³. The system configuration in Athens includes 16 boreholes, while their number increases to 24 in Copenhagen due to the higher space heating demand.

6.2.4 Monthly results

The numerical results are processed and summed, producing the monthly average COP for space heating, DHW and space cooling at both locations, which are presented in Fig. 6.16.

¹³ EC-JRC, Photovoltaic Geographical Information System (PVGIS): https://re.jrc.ec.europa.eu/pvg_tools/en/.

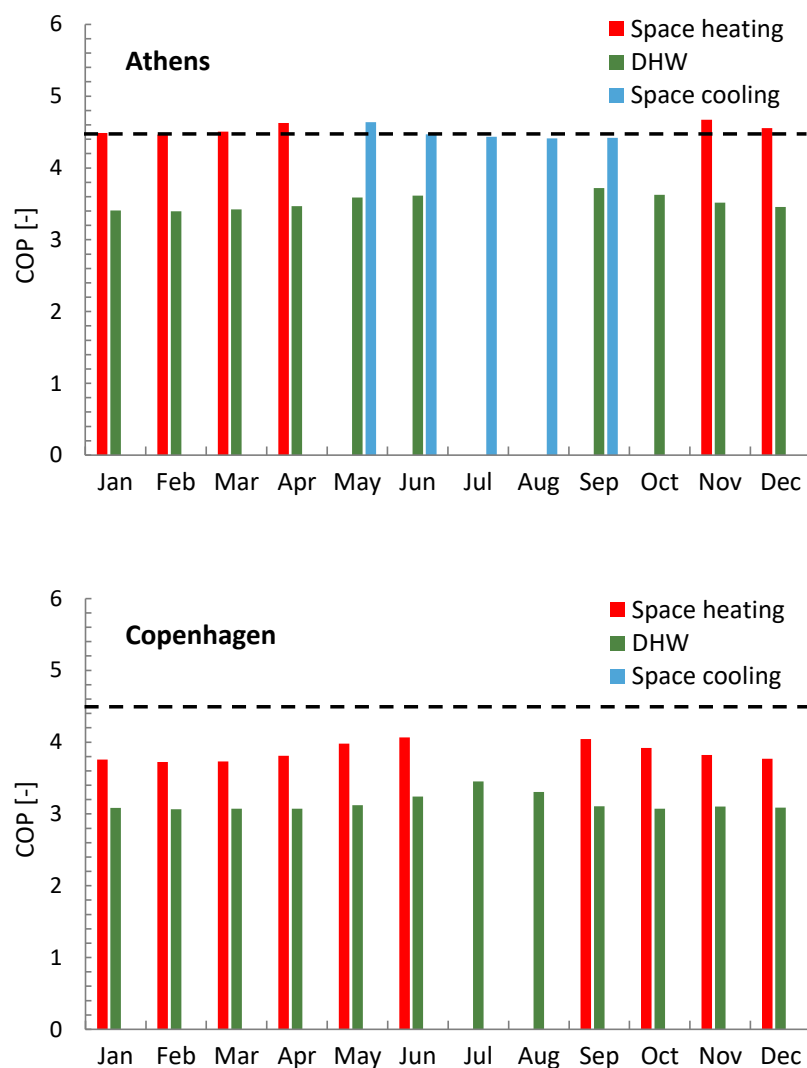


Fig. 6.16. Monthly averaged COP of the RES4BUILD system in Athens (top) and Copenhagen (bottom)

The COP for space heating and space cooling in Athens is about 4.5 during all months, while the COP for DHW is lower due to the higher temperature. On the other hand, the COP in Copenhagen is kept at a lower value due to the reduced ground temperature, which is about 10 K lower than the one in Athens.

The seasonal COP of the heat pump unit is 4.29 in Athens and 3.61 in Copenhagen, where the contribution of the heat collectors is lower. The COP per mode is presented in Table 6.3.

Table 6.3. COP per mode at the two locations

| Mode | Heat pump COP (-) | |
|-----------------------|-------------------|-------------|
| | Athens | Copenhagen |
| Space heating | 4.53 | 3.81 |
| Space cooling | 4.45 | - |
| DHW | 3.46 | 3.12 |
| Total seasonal | 4.29 | 3.61 |

The whole heating and cooling is covered using electricity, with a part of the electricity demand produced by the PVT collectors. The monthly production and consumption of the integrated system for the reference buildings at the two locations is presented in Fig. 6.17.

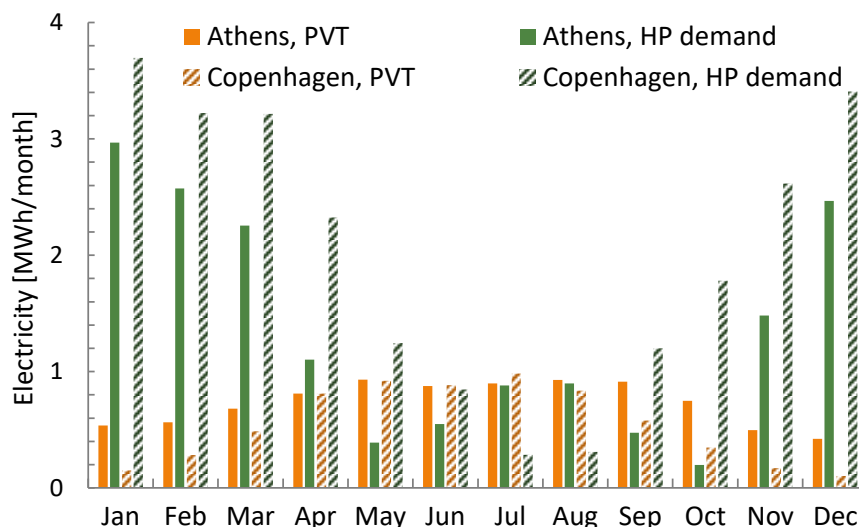


Fig. 6.17. Monthly electricity flows of the RES4BUILD system in Athens and Copenhagen

During the summer months, the PVT electricity production is the same or even higher than the heat pump system consumption at both locations. The opposite takes place during the winter months, when the heating needs are high.

6.2.5 Annual results and comparison with conventional solutions

The annual results regarding the electricity flows of the RES4BUILD system in the reference residential buildings are presented in Fig. 6.18 for both locations.

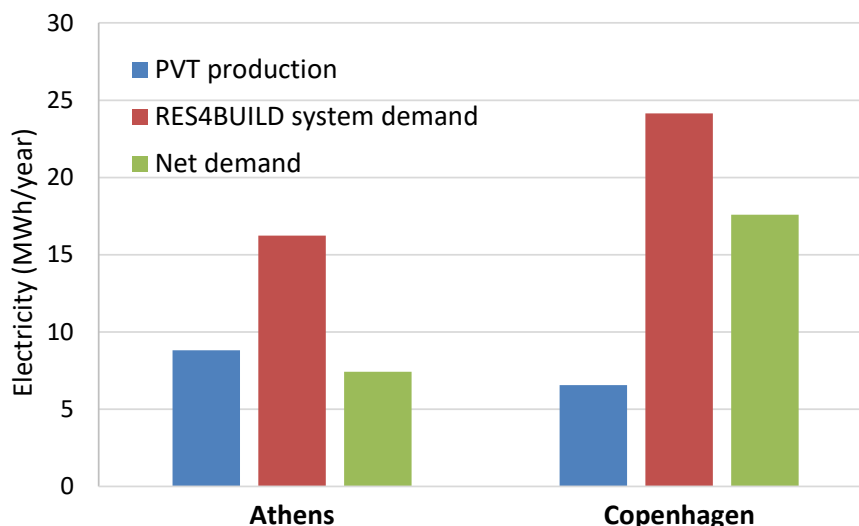


Fig. 6.18. Electricity flows of the RES4BUILD system in Athens and Copenhagen

The PVT collectors contribute to about 50 % of the demand of the heating/cooling system in Athens and 25% in Copenhagen. In case a larger number of collectors are installed or even if simple PV panels are added, this fraction increases with its upper limit constrained by the rooftop area.

The energy demand of such integrated systems is compared with a conventional system using typical efficiency parameters. This system relies on a gas boiler for heating with an efficiency of 90 % and air-

conditioning units for cooling with a seasonal COP of 2.5 for Southern European climates. An EU-average primary energy factor (PEF)¹⁴ is used equal to 2.1, with all energy flows converted to primary energy to enable a direct comparison.

The annual primary energy demands of the RES4BUILD system and a conventional system for the same reference buildings at the two locations are shown in Fig. 6.19.

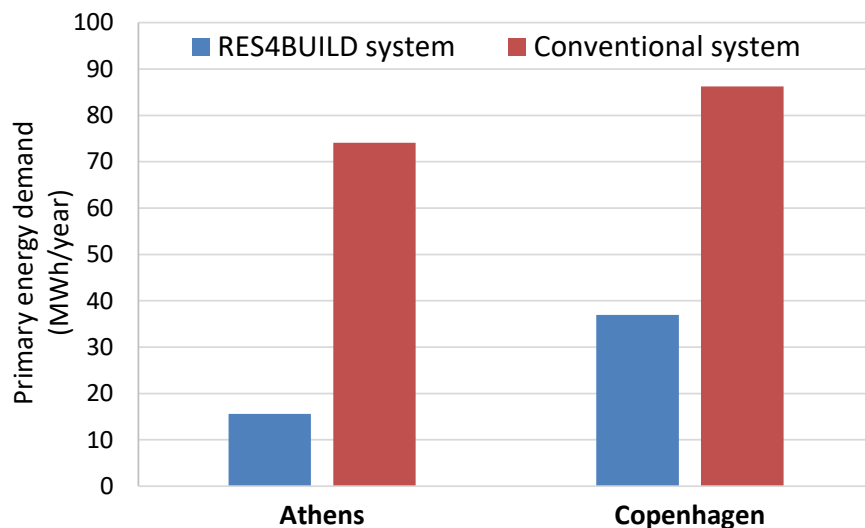


Fig. 6.19. Primary energy demand of the RES4BUILD system and a conventional system in Athens and Copenhagen

It is possible to reduce the primary energy demand of the heating/cooling system of the reference building by more than four times in Athens and two times in Copenhagen, due to the effective combination of renewable energy systems. It should be stressed here that the positive effect of the optimisation tools of WP3 are not taken into consideration, which would further reduce the primary energy demand.

Further case studies and scenarios over a wider range of building types and locations will be examined in Task 7.1 to identify the impact of the RES4BUILD solution. The analysis to be performed in WP7 will also include the control tools of WP3, with all the outcomes and results expected to be proved during the pilot system testing in WP5 for the technology validation.

¹⁴ https://www.ehpa.org/fileadmin/user_upload/201902_Joint_conversion_coefficient_paper.pdf.

7 Conclusion and next steps

The vapour compression heat pump was manufactured based on modelling results from task 2.3 and tested at NCSR D in Greece and at DTI in Denmark. The test results from NCSR D and DTI showed energy efficiencies lower than expected for the vapour compression heat pump.

Since the magnetocaloric heat pump was sensitive to the operational conditions and needed experienced supervision during operation, it was decided not to transport the magnetocaloric heat pump to DTI. The two heat pumps were to be connected in a cascade coupling and tested as one integrated heat pump. Instead, the test results of the magnetocaloric heat pump at DTU was used along with the test results of the vapour compression heat pump at DTI in a “virtual” integration, where the overall COP was calculated at different temperature scenarios. Table 7.1 shows the COPs calculated for the integrated heat pump.

Table 7.1 Calculated COPs based on test values for the integrated heat pump at different temperatures in the evaporator and condenser

| Temperature span | Calculated overall COP based on test results | Calculated Carnot efficiency |
|------------------|--|------------------------------|
| 5°C - 55°C | 1.75 | 27 % |
| 5°C - 45°C | 2.26 | 28 % |
| 5°C - 35°C | 2.76 | 27 % |

The efficiencies showed in the table are lower than those of existing heat pump solutions on the market. This results from both the magnetocaloric heat pump and the vapour compression heat pump.

The magnetocaloric heat pump efficiency has been improved during work package 2, but the technology is still at a very innovative level, and the COP of the magnetocaloric heat pump is also still low compared to fully developed technologies. The vapour compression heat pump faced component challenges that affected the efficiency results. Specifically, the efforts, which have been the focus of attention of the different teams for optimising the vapour compression heat pump, revealed that the selected compressor is not suitable to be used with the ultra-low GWP HFO refrigerant, R1234ze(E), due to the significant suction pressure drop that greatly deteriorated the COP. The decision was then to replace the compressor and the refrigerant, which required that the heat pump was shipped back to Psycrotherm to handle the necessary modifications during the summer of 2021, using a newly-available compressor series suitable for HFO blends.

Once the compressor and the refrigerant were replaced, the next step concerned the heat pump testing in Greece over a variety of conditions (e.g. a large range of evaporator and condenser water temperatures) within Task 5.3, with the aim of verifying the performance parameters, expecting to reach similar or even higher efficiency values as the one provided by the manufacturer. After that, the heat pump was shipped from Greece to DTI in Denmark in order to be part of the pilot system that will be hosted in the DTI lab within WP5 towards the validation of the RES4BUILD concept.

The test results will be used to update the heat pump model, which is a part of the system simulations. These simulations have been performed using a heat pump model corresponding to this new compressor, and they have showed that the monthly average COP is about 4.5 for both space heating and cooling in a residential building in Athens, reaching almost 4 in Copenhagen. The heat pump model is also used in the software of the controller, which is a critical part of the pilot system testing of WP5 for optimising the system operational characteristics.